pharmaceutics

MDPI

Article

Formulation Strategies to Optimize the In Vitro Release of Fenbendazole from Immediate-Release Tablets Containing Amorphous Hydroxypropyl-β-Cyclodextrin Inclusion Complexes

Ramona-Daniela Pârvănescu [1,2], Emma Adriana Ozon [3,*], Adina Magdalena Musuc [4,*], Cristina-Maria Trandafirescu [2,5], Codruța Șoica [1,2], Vasile-Adrian Surdu [6], Veronica Bratan [4], Daniela C. Culita [4], Ancuța Cătălina Fița [3] and Ion Mircioiu [7]

1 Department of Pharmacology, Physiology and Physiopathology, Faculty of Pharmacy, "Victor Babeș" 19 University of Medicine and Pharmacy, Eftimie Murgu Square No. 2, 300041 Timișoara, Romania; ramona.parvanescu@umft.ro (R.-D.P.); codrutasoica@umft.ro (C.Ș.)
2 Research Center for Experimental Pharmacology and Drug Design (X-Pharm Design), Faculty of Pharmacy, "Victor Babes" University of Medicine and Pharmacy, Eftimie Murgu Square No. 2, 300041 Timisoara, Romania; trandafirescu.cristina@umft.ro
3 Department of Pharmaceutical Technology and Biopharmacy, Faculty of Pharmacy, "Carol Davila" University of Medicine and Pharmacy, 6 Traian Vuia St., 020956 Bucharest, Romania; catalina.fita@umfcd.ro
4 Institute of Physical Chemistry—Ilie Murgulescu, Romanian Academy, 202 Spl. Independentei, 060021 Bucharest, Romania; vbratan@icf.ro (V.B.); dculita@icf.ro (D.C.C.)
5 Department of Pharmaceutical Chemistry and Biochemistry, Faculty of Pharmacy, "Victor Babeș" University of Medicine and 10 Pharmacy, Eftimie Murgu Square No. 2, 300041 Timișoara, Romania
6 Department of Materials Science, Faculty of Materials Science and Engineering, Transilvania University of Brasov, 29 Eroilor Blvd., 500036 Brasov, Romania; vasile.surdu@unitbv.ro
7 Faculty of Pharmacy, Titu Maiorescu University, 040314 Bucharest, Romania; ion.mircioiu@prof.utm.ro
* Correspondence: emma.budura@umfcd.ro (E.A.O.); amusuc@icf.ro (A.M.M.)

Abstract

Background/Objectives: The aim of this study is to obtain new inclusion complexes of fenbendazole (FEN) with hydroxypropyl-β-cyclodextrin (HP-β-CD) in order to optimize the in vitro release profile of fenbendazole from immediate-release tablets. **Methods**: Inclusion complexes and solid dispersions were prepared by coprecipitation, lyophilization, and kNeading at 1:0.25 and 1:0.5 (FEN:HP-β-CD) sub-stoichiometric molar ratios. Physical mixtures were prepared for comparison. Both physical mixtures and inclusion complexes were subsequently evaluated using physicochemical and pharmacotehnical methods. **Results**: Physicochemical analysis (FTIR, XRD, and TG/DTA) showed that lyophilization successfully induced solid-state amorphization of the drug at both ratios. Directly compressed tablets exhibited excellent mechanical properties, with crushing strength ranging from 65.1 ± 2.4 N (F3) to 87.4 ± 2.9 N (F2) and 98.2 ± 3.5 N (F1), friability below 0.7%, and rapid disintegration (58 ± 3.2 s for F1, 69 ± 4.1 s for F2, and 77 ± 4.5 s for F3). In vitro dissolution was strongly medium-dependent: at pH 1.2, cyclodextrin-based tablets achieved near-complete dissolution within 60 min (Q_{60} = 96.8 ± 2.1, DE% = 81.8 ± 1.9% for F1; Q_{60} = 99.5 ± 1.8%, DE% = 71.4 ± 2.3% for F2), compared with the uncomplexed drug (Q_{60} = 63.3 ± 2.4%, DE% = 47.5 ± 1.7% for F3). At pH 4.5 and 6.8, drug release plateaued below 15% and 38%, respectively, due to non-sink saturation constraints. **Conclusions**: This study provides in vitro proof of concept that sub-stoichiometric amorphization with HP-β-CD, coupled with direct compression, overcomes the gastric dissolution barrier of fenbendazole, establishing a solid biopharmaceutical basis for future in vivo bioavailability and stability evaluations.

Keywords: fenbendazole; HP-β-CD; inclusion complexes; dissolution kinetics

Check for updates

Academic Editor: Kyriakos Kachrimanis

Received: 19 October 2026
Revised: 13 November 2026
Accepted: 16 November 2026
Published: 18 November 2026

Copyright: © 2026 by the authors. Licensee MDPI, Basel, Switzerland. This article is an open access article distributed under the terms and conditions of the Creative Commons Attribution (CC BY) license.

1. Introduction

Fenbendazole (FEN) is a benzimidazole derivative with a broad spectrum of anthelmintic activity, widely used in veterinary medicine and actively investigated in recent years as a promising candidate for alternative oncological therapies, due to its demonstrated ability to inhibit tubulin polymerization and induce tumor cell apoptosis [1,2]. However, its clinical success via the oral route is severely limited by its unfavorable biopharmaceutical properties, with fenbendazole being variably classified in the literature as BCS Class II (low solubility, high permeability) [3] or BCS Class IV (low solubility, low permeability) [4], depending on species-specific intestinal permeability and dose-to-solubility ratios. This classification reflects its extremely low aqueous solubility—the compound is practically insoluble in biological fluids with neutral pH—and its pronounced lipophilicity, factors that make the dissolution behavior the rate-limiting step for systemic absorption and lead to erratic and low oral bioavailability [5].

Fenbendazole is a methylcarbamate benzimidazole anthelmintic characterized by a weakly basic imidazole moiety with an aqueous pKa of 4.05 [6]. Consequently, its ionization state is highly sensitive to gastrointestinal pH. While gastric acidity promotes protonation of the basic nitrogen, at near-neutral intestinal pH (pH 6.5–7.5) more than 99.8% of the drug molecules exist in their uncharged, hydrophobic molecular form, resulting in negligible aqueous solubility (<0.1 μg/mL).

To overcome this critical thermodynamic barrier, solid-state modification through molecular complexation has become one of the most effective strategies in modern pharmaceutical technology. Cyclodextrins, particularly the hydrophilic derivative hydroxypropyl beta cyclodextrin (HP-β-CD), offer the major advantage of incorporating the hydrophobic drug within their lipophilic cavity while exposing peripheral hydroxyl groups to the surrounding aqueous environment [7]. During lyophilization, the highly organized crystalline network of FEN is effectively disrupted, generating a stable molecular dispersion or an amorphous complex that eliminates the lattice energy required for dissolution and substantially improves the initial wettability of the powder at the site of contact with gastrointestinal fluids [3].

The transition from the lyophilized powder complex to a final solid pharmaceutical form, such as tablets, introduces additional technological challenges in maintaining rapid release kinetics after compaction. Formulation of immediate-release tablets requires rigorous selection of fillers and superdisintegrants capable of generating high internal hydrostatic pressure to counteract the cohesive forces exerted during compression. Traditionally, increased mechanical strength of tablets is associated with slower disintegration, but the integration of amorphous HP-β-CD matrices can trigger a remarkable synergistic effect, in which enhanced capillarity and wicking compensate for reduced porosity and accelerate structural disintegration of the solid core [8].

The main objective of this study was to develop, characterize the physicomechanical properties, and conduct an in vitro biopharmaceutical evaluation of immediate-release tablets based on fenbendazole complexed with HP-β-CD. The study aims to comparatively analyze the influence of different inclusion ratios of the complex on hardness, friability, and disintegration time, and to correlate these physical properties with dissolution kinetic profiles evaluated in environments with different physiological pH values, namely pH 1.2, pH 4.5, and pH 6.8. Through this systematic approach, the work aims to develop and evaluate delivery systems capable of substantially improving the gastric dissolution rate of fenbendazole, providing an in vitro biopharmaceutical rationale that may facilitate oral drug absorption.

While prior studies have investigated fenbendazole in hot-melt extruded polymeric dispersions [3] or simple solution cyclodextrin complexes [9,10], this work addresses the

translational gap between lyophilized amorphous cyclodextrin powders and finished solid dosage forms. Specifically, this study couples sub-stoichiometric HP-β-CD amorphization with direct-compression tableting, elucidating the interplay between tableting forces, superdisintegrant wicking kinetics, and multi-pH dissolution in physiologically distinct media. The study demonstrates that even a modest affinity complex can drastically enhance gastric dissolution in a highly scalable tablet matrix.

2. Materials and Methods

2.1. Materials

Fenbendazole (FEN, active pharmaceutical ingredient, Batch #20230512, certified purity 99.4% by HPLC) was provided by Shaanxi Hanjiang Pharmaceutical Group Co., Ltd. (Hanzhong City, China). Hydroxypropyl-β-cyclodextrin (HP-β-CD, pharmaceutical grade, Batch #BCCF8921) was purchased from Sigma-Aldrich Chemie GmbH (Steinheim, Germany); the polymer is characterized by an average molecular weight of M*w*~1460 g/mol and an average molar substitution degree (MS) of 0.65 (~4.5–5.0 hydroxypropyl groups per cyclodextrin molecule).

Avicel® pH 102 was purchased from International Flavors and Fragrances Inc. (IFF, New York, NY, USA). The superdisintegrant EXPLOTAB® was provided by JRS PHARMA GmbH & Co. KG (Rosenberg, Germany), and the lubricant LIGAMED® MF-2-V was provided by Peter Graven NV (Gelderland, The Netherlands).

All chemicals and solvents used during the experimental stages were of high purity and analytical grade. The active components and auxiliary materials were weighed precisely using a high-resolution analytical balance, model Mettler Toledo AT261 (Mettler Toledo, Greifensee, Switzerland), with a sensitivity of 0.01 mg.

2.2. Methods

2.2.1. Solubility Studies

Molar Absorptivity of the FEN Active Substance

To determine the molar absorptivity of FEN, solutions with various molar concentrations in DMSO were prepared. The absorbances of the resulting solutions were measured as a function of DMSO, using a UV-Vis Perkin-Elmer Lambda 35 spectrophotometer (Shelton, CT, USA). The experiments were conducted in triplicate.

Phase-solubility studies were conducted according to the method described by Higuchi and Connors [11]. A 0.1006 M stock solution of HP-β-CD was prepared by dissolving 2.061 g of HP-β-CD in 15 mL of distilled water under magnetic stirring using a HeidolpH MR 3001 K magnetic stirrer (Schwabach, Germany). Serial dilutions were prepared in distilled water to obtain six increasing cyclodextrin concentrations (0 to 0.1006 M). An excess amount of FEN (10 mg) was added to each 5 mL solution in sealed glass vials. The suspensions were equilibrated in a thermostatic shaking water bath at 25.0 ± 0.5 °C for 48 h to ensure that thermodynamic dissolution equilibrium was fully attained. Following equilibration, the samples were filtered through 0.45 µm nylon membrane syringe filters (discarding the first 2 mL of filtrate). The filtered solutions were diluted with DMSO/water (50:50 *v*/*v*) to eliminate turbidity, and absorbance was recorded at 298 nm (corresponding to the bathochromically shifted absorption maximum of fenbendazole in the presence of DMSO) using a Perkin-Elmer Lambda 35 UV-Vis spectrophotometer. All determinations were performed in triplicate ($n = 3$).

2.2.2. Manufacturing Process of the Binary Systems

The FEN-HP-β-CD binary systems were prepared in two molar ratios (1:0.5 and 1:0.25) using different techniques: two liquid-phase methods (coprecipitation and lyophilization) and two solid-phase methods (kneading and physical mixing). To determine which technique ensures complete molecular inclusion of the active ingredient in the HP-β-CD cavity, the binary systems were characterized by Fourier transform infrared spectroscopy (FTIR), simultaneous thermogravimetric and differential thermal analysis (TG/DTA), and powder X-ray diffraction (XRD). The results were evaluated in comparison with those of the pure starting materials.

The reported ratios (1:0.25 and 1:0.5) represent the initial preparation ratios. Substoichiometric molar ratios were strategically selected to balance the solubilizing benefit of HP-β-CD with the stringent mass constraints of the final tablet (500 mg).

For the liquid-phase methods, the components were initially weighed separately. FEN was dissolved in acetone, and HP-β-CD was dissolved in distilled water. The aqueous cyclodextrin solution was gradually added to the FEN solution, and the mixtures were subjected to mechanical agitation at 1000 rpm using a HeidolpH MR 3001 K magnetic stirrer at room temperature for 8 h. In the coprecipitation technique, the resulting suspensions were filtered, and the isolated sediments were dried at 25 °C for 24 h. For the lyophilization technique, the homogenized mixtures were frozen and then lyophilized at −60 °C for 18 h using a CoolSafe Basic and Pro lyophilizer produced by Labogene A/S, Allerod, Denmark. Upon completion of the freeze-drying cycle, the collected lyophilized cakes were gently pulverized, immediately transferred into airtight amber glass containers, and stored in a vacuum desiccator containing freshly activated silica gel at controlled room temperature (20 ± 2 °C) in the dark until further processing into direct compression blends.

In the kNeading method, specified amounts of FEN and HP-β-CD were weighed and kNeaded for 2 h in a mortar with a small amount of a 50:50 v/v mixture of ethyl alcohol and water. The resulting consolidated mass was passed through a 12-mesh sieve, and the collected granules were dried at 25 °C for 24 h, then ground to a fine powder.

Evaluation of manufacturing efficiency showed superior process yields for lyophilization (96.8 ± 1.4% for the 1:0.25 and 95.5 ± 1.8% for the 1:0.5 molar ratio), followed by the kNeading method (88.2 ± 2.6% and 86.9 ± 2.1%, respectively), whereas coprecipitation produced markedly lower recoveries (68.4 ± 3.7% and 64.1 ± 3.1%), primarily due to active ingredient loss in the supernatant during the precipitation and filtration stages.

For the preparation of the physical reference mixtures, the substances were weighed according to the same molar ratios and manually homogenized in a mortar for 2 min at room temperature to ensure uniform distribution of the components.

2.2.3. Physicochemical Evaluation

FTIR spectra were recorded using a Jasco FT/IR 4700 spectrophotometer (Jasco, Easton, MD, USA) with samples prepared as KBr pellets. Simultaneous thermogravimetric analysis and differential thermal analysis (TG/DTA) were carried out using a NETZSCH STA 449 F3 Jupiter instrument (Selb, Germany) over a temperature range of 25–600 °C. Samples (~5 mg) were placed in open aluminum oxide crucibles and heated at a constant heating rate of 10 °C/min under a dynamic nitrogen atmosphere (flow rate: 20 mL/min). The DTA signal was utilized to track thermal phase transitions (melting and crystallization phenomena), while TG monitored associated mass loss events. XRD measurements were registered on a Bruker D8 Advance diffractometer (Bruker, Billerica, MA, USA) using Ni-filtered Cu-Kα radiation (λ = 1.5418 Å), which operated at 40 kV and 40 mA. The diffractograms were recorded in the 2θ = 5–60° range, with a step size of 0.02°.

2.2.4. Preformulation and Formulation Design of FEN-HP-β-CD Tablets

Since physicochemical investigations of the inclusion complexes showed that the lyophilization technique provides the highest solid-state amorphization and complexation efficiency of FEN in the HP-β-CD cavity, this type of system was selected as the active pharmaceutical ingredient for tablet development. Although the amorphous structure of the lyophilized complexes has a clear positive effect on the dissolution profile and biopharmaceutical performance, it is well documented that this solid state leads to deficiencies in the rheological and compressible properties of the powders. These technological attributes are fundamentally important in tablet production, playing a critical role in direct compression operations.

To prevent exposure of the active ingredients to thermal and water degradation, direct compression is considered superior to the wet granulation technique. However, industrial processing of lyophilized material presents major technical challenges, requiring careful design of both the qualitative and quantitative composition, along with strict optimization of technological parameters. Therefore, the rational selection of excipients is a pivotal step in the design phase of the pharmaceutical form, as achieving optimal flow and compaction characteristics of the powder mixture is essential to ensure the reproducibility and high quality of the final solid pharmaceutical forms [11,12].

2.2.5. Formulation of the Powder Mixtures for Direct Compression

The formulation stage for mixtures intended for direct compression involved a rigorous selection of pharmaceutical excipients with specific functions to ensure rapid disintegration and dissolution of the solid matrix. The proportions of the inclusion complexes and auxiliary materials were established to guarantee an exact therapeutic dose of 100 mg of FEN per tablet unit and a total mass of 500 mg for each tablet.

The qualitative and quantitative composition of these powder systems is presented in Table 1, which highlights that the experimental formulation coded F1 contains the 1:0.5 FEN-HP-β-CD inclusion complex, F2 contains the 1:0.25 FEN-HP-β-CD inclusion complex, and F3 contains only FEN.

Table 1. Formulation of the powder mixtures for direct compression.

Ingredient	Formulation/Amount (%)		
	F1	**F2**	**F3**
FEN-HP-β-CD 1:0.5 lyophilized complex system	68.80	-	-
FEN-HP-β-CD 1:0.25 lyophilized complex system	-	44.40	-
FEN	-	-	20
Avicel® pH 102—microcrystalline cellulose	28.20	52.60	77.00
EXPLOTAB®—Sodium starch glycolate	2.00	2.00	2.00
LIGAMED® MF-2-V—Magnesium stearate	1.00	1.00	1.00
TOTAL	100.00	100.00	100.00

Avicel pH 102 is a high-quality grade of microcrystalline cellulose and is considered a reference excipient in the pharmaceutical industry due to its multifunctional profile. It serves as a binder, filler, disintegrant, and flow promoter in the formulation of tablets. Structurally and chemically, it is defined as a purified, partially depolymerized cellulose. Its widespread use in pharmaceutical technology is based on its excellent compressibility and flow properties, which are critical for optimizing compression processing parameters and ensuring the mechanical integrity of the solid pharmaceutical forms [13].

Sodium starch glycolate was chosen for its superdisintegrant properties. Its mechanism of action relies on its exceptional hydrophilic capacity, which enables it to rapidly absorb water upon contact with gastrointestinal fluids, causing intense macromolecular swelling. This rapid volumetric expansion creates high internal pressure that quickly disassembles the tablet's solid matrix, facilitating the dissolution and efficient release of the active ingredients [14,15].

Magnesium stearate functions as a lubricant and flow promoter, and was selected to optimize the rheological profile of mixtures by preventing agglomeration of powder particles.

2.2.6. Manufacturing of the Powder Mixtures for Direct Compression

The process of preparing the mixtures for direct compression began with preliminary sieving of all ingredients through a standardized 20-mesh sieve to ensure granulometric calibration and eliminate any agglomerates. After this step, the components were weighed precisely and homogenized (except for magnesium stearate) for 10 min. This operation was performed at room temperature using a Plexiglas cubic mixer, type CMP 12, produced by Pharmag GmbH (Klipphausen, Germany), set at a constant rotation speed of 30 rpm. Finally, magnesium stearate was added, and the final blend was stirred under the same conditions for two more minutes.

2.3. Characterization of the Pharmacotechnical Profile of Powder Mixtures

All experimental determinations were performed in three independent replicates for each material sample, ensuring the reproducibility and statistical representativeness of the data.

The particle size distribution of the powders was evaluated by analytical sieving, using an electromagnetic shaker, CISA Sieve Shaker Mod. RP 10, produced by Cisa Cedaceria Industrial (Barcelona, Spain). The protocol involved transferring 50 g of each material onto a column of standardized sieves, arranged vertically in increasing order of mesh opening and subjected to vibration. The sieve column consisted of calibrated sieves according to ISO 3310-1: 800, 600, 400, 315, 250, 160, 125, and 80 µm. The vibration amplitude was maintained at 1.5 mm for 20 min. After 20 min of continuous shaking, the powder fraction retained on each sieve was quantitatively collected and weighed with precision, enabling mathematical modeling of the particle size profile in the mixtures for direct compression [11].

The moisture content of the powder mixtures was evaluated using a thermogravimetric method, based on the quantitative determination of the loss on drying of the material under analysis. A high-precision halogen moisture analyzer, model HR 73 Mettler Toledo (Mettler-Toledo GmbH, Greifensee, Switzerland), was operated at a constant temperature of 105 °C. Approximately 2.0 g of powder was spread evenly on the sample pan, and drying was carried out until an automated switch-off endpoint criterion was reached, defined as a mass loss rate of less than 1.0 mg within 90 s. This investigation is essential in the preliminary characterization of powders, as controlling residual moisture directly influences the flow properties, compaction capacity of the solid matrix, and long-term physicochemical stability of the tablets.

The flowability of powder mixtures was assessed by measuring the angle of repose, flow time, and flow rate. The experimental protocol involved processing 60 g of each powder and recording the parameters during the free passage of the material through an orifice with a calibrated diameter. Measurements were performed using an automated powder and granulate analysis system, model PTG-S3, manufactured by Pharma Test Apparatebau GmbH (Hainburg, Germany). Monitoring these dynamic and geometric indices is particularly important in pharmaceutical technology, as it provides essential predictive data on the flowability of the mixture during gravitational feeding of the dies and ensures the consistency of the mass of the dosed units.

The compressibility of powder mixtures was evaluated by analyzing their volumetric characteristics using a Vankel Tap Density Tester (Vankel Industries Inc., Cary, NC, USA). The experimental protocol involved introducing 50 g of each powder, without prior compaction, into a dry graduated cylinder, followed by an immediate reading of the initial apparent volume. The cylinder was then subjected to a predefined number of mechanical shocks to determine the degree of compaction volumetrically. Based on these parameters, the initial apparent density, the density after compaction, the Hausner index (HR), and the Carr compressibility index (CI) were calculated. The Hausner index is defined as the ratio of the density after compaction to the initial apparent density, while the Carr index was determined according to the standard mathematical Equations (1) and (2).

$$HR = \frac{\rho_{tapped}}{\rho_{bulk}} \quad (1)$$

$$CI(\%) = 100 \times \frac{\left(\rho_{tapped} - \rho_{bulk}\right)}{\rho_{tapped}} \quad (2)$$

where ρ_{tapped} is the tapped bulk density of the blend (g/cm^3) and ρ_{bulk} is the loose bulk density of the material (g/cm^3).

For materials for direct compression processing, reference values require the Hausner index to be below 1.25 and the Carr index to be below 10 to ensure free flow and optimal compressibility [16].

2.4. Design and Evaluation of Tablets Containing FEN

2.4.1. Tablet Formulation

After evaluating the results from the preliminary preformulation tests, all three powder mixtures designed for direct compression showed pharmacotechnical properties suitable for the technological requirements of tablet processing. The qualitative and quantitative composition of these oral therapeutic systems is detailed in Table 2.

Table 2. FEN tablets composition.

Ingredient	Quantity mg/Tablet			Role in Formulation
	F1	F2	F3	
FEN-HP-β-CD 1:0.5 lyophilized complex system	344	-	-	Active ingredient
FEN-HP-β-CD 1:0.25 lyophilized complex system	-	222	-	Active ingredient
FEN	-	-	100	Active ingredient
Avicel® pH 102—microcrystalline cellulose	141	263	385	Filler Binder
EXPLOTAB®—Sodium starch glycolate	10	10	10	Superdisintegrant
LIGAMED® MF-2-V—Magnesium stearate	5	5	5	Lubricant
TOTAL	500	500	500	

2.4.2. Tablet Manufacturing

The powder mixtures were compacted by applying an average compression force of 30 kN using a single-station eccentric tablet press, model Erweka EP-1 (Erweka, Germany). The device was equipped with 13 mm diameter flat-faced punches, and the operating parameters were precisely adjusted to produce tablets with an average mass of 500 mg. This technological calibration ensured the delivery of an accurate therapeutic dose, corresponding to a weight content of 100 mg of FEN per tablet.

2.4.3. Tablet Quality Evaluation

All tablets obtained were subjected to rigorous characterization in accordance with the recommendations of the current compendium [17].

The dimensional profile of the tablets was evaluated by accurately determining their diameter and thickness. Measurements were performed on a sample of ten tablets from each experimental series using the digital hardness tester VK 200 Tablet Hardness Tester (Vanderkamp, Edison, NJ, USA), ensuring monitoring of the geometric uniformity of the tablets.

To verify ***mass uniformity*** after the compression process, 20 tablets from each batch were weighed individually. The average mass was calculated, and the percentage deviations from the theoretical value were evaluated according to official control protocols [17].

Drug content and uniformity of dosage units were evaluated in accordance with Ph. Eur. guidelines [17]. Ten individual tablets from each experimental batch were accurately weighed, pulverized in an agate mortar, and quantitatively transferred to 100 mL volumetric flasks containing acidified methanol (0.1 N HCl in methanol). The suspensions were extracted under continuous magnetic stirring and ultrasonic treatment for 30 min to ensure complete drug dissolution. After extraction, the mixtures were filtered through 0.45 µm nylon syringe filters, appropriately diluted with dissolution medium, and analyzed spectrophotometrically at 288 nm. The percentage of active ingredient relative to the nominal dose (100 mg FEN) was determined for each unit, and the acceptance value (AV) was calculated to verify content uniformity.

Mechanical resistance to fracture was evaluated on batches of 10 tablets from each series using the same automated VK 200 equipment. Each tablet was positioned diametrically between the two anvils of the device and subjected to a progressively increasing compression force applied by the mobile brace. The recorded reference value was the minimum force required to induce the initial fracture of the tablet.

Friability was determined on samples of 10 tablets for each formulation using a Vankel friabler. The tablets were dedusted, accurately weighed, placed in the rotating drum of the device, and subjected to 100 revolutions (25 rpm for 4 min). After the cycle, the tablets were carefully dedusted to remove any adhering powder and reweighed. The mass loss was calculated and expressed as a percentage. For the formulations to be considered technologically compliant, the value must not exceed the critical threshold of 1.0% [17].

The disintegration behavior was evaluated on a sample of six tablets for each experimental formulation, in accordance with the relevant compendial recommendations [17]. Testing was conducted in distilled water maintained at a constant physiological temperature of 37 ± 0.5 °C, using an Erweka DT 3 disintegration time determination device manufactured by Erweka® GmbH (Langen, Germany). The time interval, expressed in seconds, required for complete disintegration of the tablets in the test medium was monitored and recorded.

In Vitro Drug Release Studies

Drug release profiles of the fenbendazole formulations (100 mg dose) were evaluated using an Erweka DT 800 dissolution tester configured with USP Apparatus II (paddles). Dissolution runs were carried out at 37.0 ± 0.5 °C and 75 rpm. Each vessel contained 900 mL of dissolution medium, and three media spanning the physiological gastrointestinal pH range were assessed: 0.1 N hydrochloric acid at pH 1.2 (simulating gastric fluid), sodium acetate buffer at pH 4.5 containing 0.2% SDS, and phosphate buffer at pH 6.8 without surfactant (approximating the near-neutral intestinal environment).

Aliquots were withdrawn at 5, 10, 15, 20, 30, 45, and 60 min; after each withdrawal, an equivalent volume of fresh, preheated medium was added to maintain the hydrodynamic volume. All withdrawn aliquots were immediately filtered through 0.45 µm nylon membrane syringe filters, discarding the first 2 mL of filtrate, to prevent optical interference from

undissolved, suspended drug particles during spectrophotometric quantification. Filter adsorption was systematically evaluated by passing standard FEN solutions (5, 10, and 20 µg/mL) through 0.45 µm nylon membrane syringe filters. After discarding the initial 2 mL of filtrate, drug recovery was 99.1 ± 0.8% relative to unfiltered, centrifuged aliquots, confirming no loss due to membrane adsorption. All dissolution runs were performed in triplicate ($n = 3$), and results are expressed as mean ± standard deviation (SD).

FEN is a weakly basic, highly lipophilic drug (pK_a ≈ 4.0, log $p \approx 3.8$). In strongly acidic gastric media (pH 1.2), FEN is largely protonated, resulting in higher intrinsic solubility. In intermediate media (pH 4.5), unionized FEN has negligible aqueous solubility; 0.2% w/v SDS was added to mimic physiological wetting and partial micellar solubilization (the surfactant action of bile salts) to examine whether sink conditions could be approached. Surfactant-free phosphate buffer (pH 6.8) was used to evaluate intrinsic, unassisted dissolution under simulated distal intestinal conditions.

UV Spectrophotometric Analysis

FEN was quantified spectrophotometrically by UV detection at 288 nm. The dissolved fraction in each withdrawn sample was determined against calibration standards of fenbendazole prepared in the corresponding dissolution medium, enabling accurate calculation of the cumulative percentage of drug released at each sampling point.

The UV spectrophotometric quantification method was validated in accordance with ICH Q2(R1) guidelines in all three dissolution media. The method showed high linearity over the concentration range of 1.0–25.0 µg/mL ($r^2 \geq 0.9992$ in all media). Satisfactory precision was demonstrated with repeatability (%RSD < 1.4%) and intermediate precision (%RSD < 1.9%). Accuracy assessed at three concentration levels yielded recoveries ranging from 98.4% to 101.6%. Method specificity was confirmed using placebo compact extracts (containing Avicel® pH 102, Explotab®, and magnesium stearate), which produced negligible background absorbance at 288 nm (A < 0.008 AU), indicating no interference from excipients or buffer.

Release profiles were further compared using model-independent metrics, namely dissolution efficiency ($DE\%$) and mean dissolution time (MDT). Dissolution efficiency ($DE\%$) was calculated as the area under the dissolution curve up to time t ($t = 60$ min), expressed as a percentage of the area of the rectangle described by 100% dissolution over the same time period, according to the method of Khan and Rhodes [18]:

$$DE\% = \frac{\int_0^T y \cdot dt}{y_{100} \cdot T} \times 100 \quad (3)$$

where y is the percentage of drug dissolved at time t, and y_{100} represents 100% dissolution. The integral was computed numerically using the trapezoidal rule.

Mean dissolution time (MDT), which characterizes the drug release rate and reflects the residence time of the drug inside the matrix prior to release, was determined according to Möckel and Lippold [19] using the equation

$$MDT = \frac{\sum_{i=1}^{n} \bar{t}_i \cdot \Delta M_i}{\sum_{i=1}^{n} \Delta M_i} \quad (4)$$

where i is the dissolution sample number, n is the total number of sampling points, $\bar{t}_i = (t_i + t_{i-1})/2$ is the midpoint of the time interval between t_i and t_{i-1}, and ΔM_i is the additional percentage of drug dissolved during that specific time increment.

The saturation solubility (C_s) of fenbendazole was determined in triplicate by adding excess drug to 20 mL of each dissolution medium at 37.0 ± 0.5 °C under continuous shaking for 48 h, followed by filtration through a 0.45 µm membrane and UV quantification. The sink index (S) was calculated using the equation

$$S = \frac{C_s \cdot V}{\text{Dose}} \quad (5)$$

where (V) is the medium volume (900 mL) and Dose is 100 mg.

The difference factor (f1) and similarity factor (f2) were calculated according to FDA [20] and EMA [21] guidelines to compare each cyclodextrin formulation (F1, F2) with the crystalline drug tablet (F3). To meet regulatory guidelines, only one measurement point after 85% dissolution was included in the comparison (up to 30 min for pH 1.2), and percent coefficients of variation (%CV) among vessels were confirmed to be below 20% at earlier time points and below 10% thereafter.

2.5. Statistical Analysis

Data are expressed as mean ± standard deviation (SD). Differences among formulations (F1, F2, F3) in hardness, disintegration time, DE%, MDT, and Q_{60} were evaluated using one-way analysis of variance (ANOVA) followed by Tukey's honestly significant difference (HSD) post hoc test. Normality was assessed with the Shapiro–Wilk test, and homogeneity of variances with Levene's test. A p-value < 0.05 was considered statistically significant.

3. Results and Discussion

3.1. Phase-Solubility Diagrams

Phase-solubility studies, which examine the influence of cyclodextrin concentration on the solubility of a poorly soluble species, FEN in our case, provide a rapid and reliable method for investigating the potential formation of inclusion complexes. The parameters derived from the phase-solubility diagram obtained according to the method of Higuchi and Connors [22,23] were subsequently used to estimate the stoichiometric ratio and calculate the formation constant of the inclusion complexes. Phase-solubility studies typically precede the preparation of inclusion complexes, as they provide definitive information regarding both the formation of the complexes and their composition. The calibration curve using the reference solution (FEN in DMSO) is represented in Figure 1a. The phase-solubility diagram obtained based on the Higuchi and Connors method was represented in Figure 1b. Assuming that the inclusion complex was formed in a 1:1 stoichiometric ratio, the following Equations (6) and (7) were used to calculate the apparent stability constant (K_{st}) and the complexation efficiency (CE):

$$K_{st} = \frac{slope}{S_o(1 - slope)} \quad (6)$$

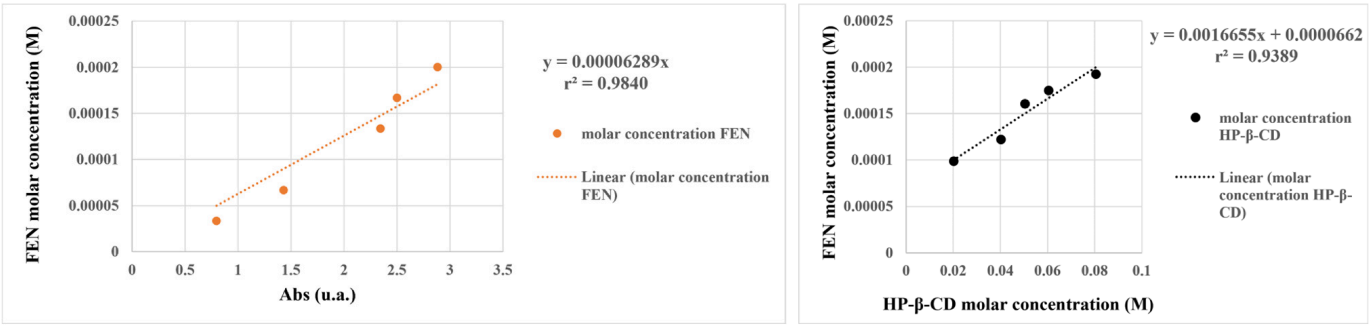
$$CE = \frac{\text{Slope}}{1 - \text{Slope}} = K_{st} \cdot S_0 \quad (7)$$

where K_{st} is the apparent stability constant of the 1:1 inclusion complex, and S_o is the intrinsic solubility of FEN without HP-β-CD (assessed from the intercept of the phase-solubility curve) [22,24].

The phase-solubility diagram of fenbendazole in aqueous HP-β-CD solutions (Figure 1b) showed a classic A_L-type linear profile ($r^2 = 0.9912$) with a slope significantly below unity (slope = 0.00166). This linear dependence indicates that soluble inclusion complexes were formed predominantly with a 1:1 stoichiometric host–guest ratio over the investigated cyclodextrin concentration range. The intrinsic aqueous solubility of FEN (S_o) extrapolated from the y-intercept was 6.62×10^{-5} M (~19.8 µg/mL). Based on these parameters, the apparent stability constant was determined to be $K_{st} = 25.2\ M^{-1}$, with a corresponding complexation efficiency of 0.00167.

A stability constant of 25.2 M^{-1} reflects a relatively modest binding affinity in aqueous solution compared with strongly interacting lipophilic drugs ($K_{st} > 100$–$1000\ M^{-1}$) [25]. This thermodynamic value indicates that solubilization in solution is primarily driven by

cyclodextrin mass action equilibria rather than exceptionally tight host–guest entrapment. Furthermore, given the high molecular weight of HP-β-CD (~1460 g/mol) relative to fenbendazole (299.35 g/mol), achieving a stoichiometric 1:1 molar complex in the solid state would require 487.7 mg of cyclodextrin per 100 mg drug dose. This would yield an intermediate complex mass of nearly 588 mg, making the manufacture of a standard acceptable 500 mg oral tablet unfeasible before adding essential compaction fillers and disintegrants. Consequently, sub-stoichiometric ratios of 1:0.25 and 1:0.5 (FEN:HP-β-CD) were deliberately selected for solid-state processing. In these systems, the predominant mechanism driving dissolution enhancement is not complete, rigid molecular encapsulation, but rather the formation of amorphous solid dispersions containing partial inclusion complexes, where elimination of the drug crystal lattice and hydrophilic surface wetting collectively overcome the dissolution barrier.



(**a**) (**b**)

Figure 1. (**a**) Calibration curve; (**b**) the phase-solubility diagram of FEN–HP-β-CD system.

3.2. Physicochemical Evaluation

FTIR spectra of FEN, HP-β-CD, FEN-HP-β-CD 1:0.25 physical mixture, FEN-HP-β-CD 1:0.5 physical mixture and their inclusion complexes obtained using the coprecipitation, lyophilization and kNeading methods are shown in Figure 2. The FTIR technique was used to evaluate the interaction between FEN and HP-β-cyclodextrin (1:0.25 and 1:0.5 molar ratios) in their physical mixture and inclusion complexes obtained using the three preparation methods: coprecipitation, lyophilization, and kNeading.

The FTIR spectrum of FEN from Figure 2a shows the characteristic absorption peaks of the pure compound: at 3340 cm^{-1}, the absorption peak is assigned to N-H stretching from amide; the peak at 3055 cm^{-1} is assigned to aromatic C-H stretching, which corresponds to the benzene ring. The C=O stretching vibration is observed around 1627 cm^{-1} and the C-N group from benzimidazole is observed at around 1267 cm^{-1} [5,26–28]. The FTIR spectrum of HP-β-CD (Figure 2b) showed the main characteristic vibration peaks, which correspond to polysaccharide types: the peak at 3400 cm^{-1} is attributed to O-H stretching vibration; at 2929 cm^{-1}, the peak is due to C-H stretching vibration; at 1645 cm^{-1}, the peak is attributed to H-O-H bending vibration; and the peak at 1030 cm^{-1} is attributed to C-O bond vibration [29,30].

In the physical mixtures (Figure 2c,g) corresponding to the two molar ratios, the FTIR spectra showed only an overlap of the contributions from the two components (FEN and HP-β-CD), and the intensities are influenced by their proportions. A reduction in the intensity of the FEN bands in the compound with a 1:0.5 molar ratio results only from its dilution with HP-β-CD. The physical mixture does not demonstrate the formation of a complex.

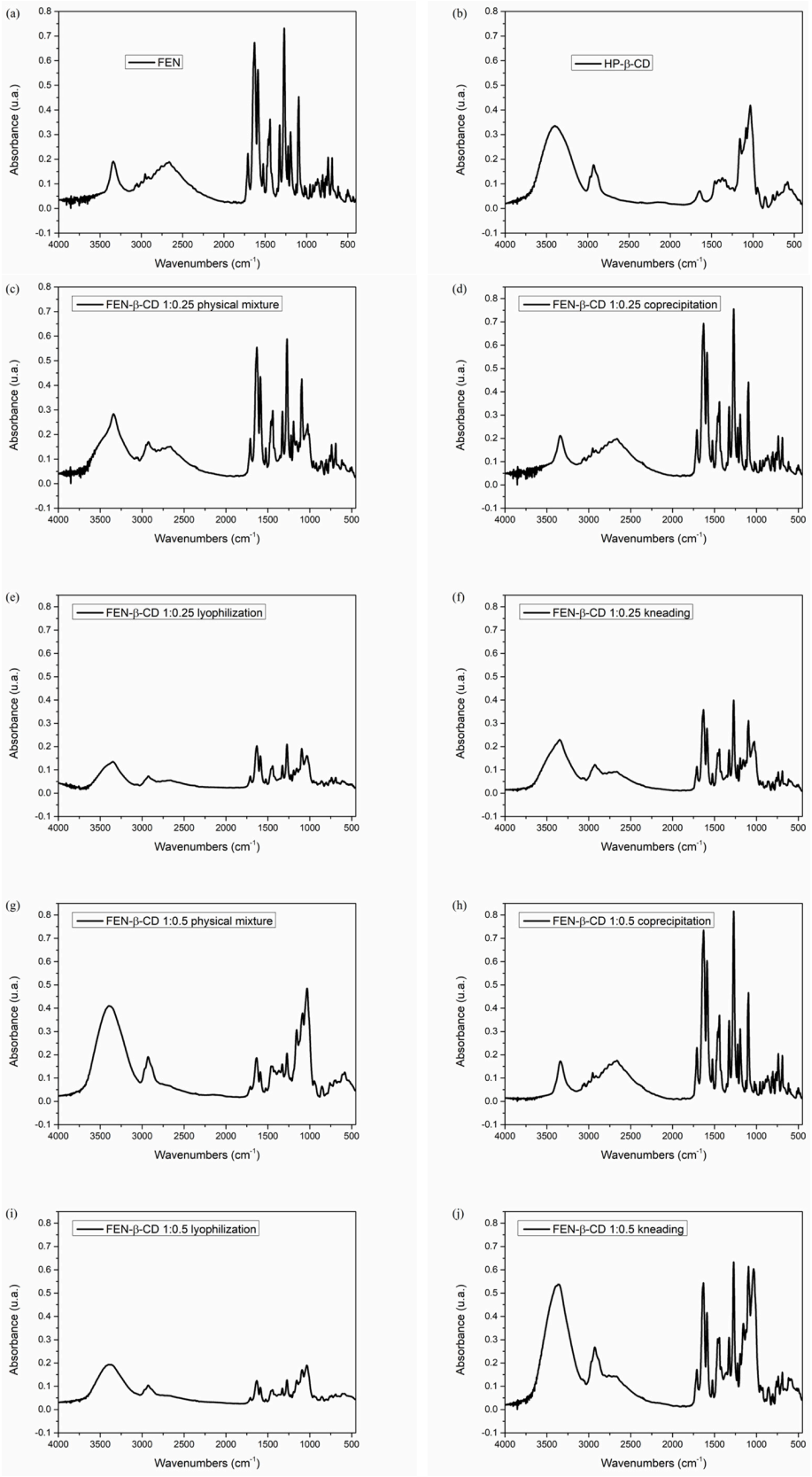


Figure 2. FTIR spectra of (**a**) FEN; (**b**) HP-β-CD; (**c**) physical mixture between FEN and HP-β-CD in 1:0.25 molar ratio and its inclusion complexes; (**d**) FEN-HP-β-CD coprecipitation; (**e**) FEN-HP-β-CD lyophilization and (**f**) FEN-HP-β-CD kNeading; (**g**) physical mixture between FEN and HP-β-CD in 1:0.5 molar ratio and its inclusion complexes; (**h**) FEN-HP-β-CD coprecipitation; (**i**) FEN-HP-β-CD lyophilization and (**j**) FEN-HP-β-CD kNeading.

The FTIR spectra of FEN–HP-β-CD inclusion complexes using two molar ratios of 1:0.25 and 1:0.5 revealed some differences depending on the preparation method (coprecipitation, lyophilization, and kNeading method). For both molar ratios, the lyophilization method led to the most pronounced spectral changes, with the disappearance of the characteristic FTIR absorption bands of FEN and HP-β-CD. These modifications suggest changes in the molecular environment of FEN and potential intermolecular interactions with HP-β-CD, supporting the hypothesis that inclusion complexes are formed for both molar ratios. In contrast, the inclusion complexes obtained via coprecipitation and kNeading methods retained some of the absorption bands characteristic of the individual components, indicating that some of their molecular vibrations remained pronounced. However, the FTIR spectra of the products formed by the coprecipitation and kNeading methods are different related to the original pure compounds, proving that complexation takes place in these complexation techniques. Overall, the FTIR results suggest that the preparation method influences the interactions between FEN and HP-β-CD, with the freeze-drying method inducing the most significant spectral changes for both investigated molar ratios. The same findings are observed for other inclusion compounds in our previous studies [11,31].

The X-ray diffraction technique clearly shows the complete drug–cyclodextrin complexation, as indicated by a new XRD pattern different from the pure components. The X-ray diffraction patterns of FEN, HP-β-CD, their physical mixture, and FEN-HP-β-CD in 1:0.25 and 1:0.5 molar ratios obtained using coprecipitation, lyophilization, and kNeading methods are shown in Figure 3.

The X-ray diffraction spectrum of FEN (Figure 3a) showed some well-defined peaks appearing at $2\theta = 6.94, 11.45, 13.60, 18.24, 21.60, 24.31, 26.36, 31.93°$, revealing its crystalline nature [32–34]. The XRD pattern of HP-β-CD (Figure 3b) showed broad peaks around $2\theta = 9.92°$ and 19.02°, proving its amorphous structure.

Analysis of the X-ray diffraction patterns of the inclusion complexes formed by coprecipitation, lyophilization, and kNeading methods highlights the influence of the preparation method on the crystalline structure of FEN-HP-β-CD systems, for both investigated molar ratios (1:0.25 and 1:0.5). In the case of physical mixtures, the crystalline character of FEN is well maintained, as evidenced by the presence of its characteristic diffraction peaks, although their intensity is somewhat different depending on the ratio of HP-β-CD (Figure 3c,g). For the compounds obtained via coprecipitation and kNeading methods, a reduction in their crystallinity is observed, which is established by a decrease in the intensity of the diffraction peaks, while some peaks characteristic of FEN are still maintained. This behavior suggests a partial reduction in crystalline character, without the complete disappearance of the active compound. In contrast, the lyophilization method leads to the most pronounced changes in the diffraction profile, resulting in a clear transformation of the initial pattern and the disappearance of the peaks characteristic of FEN. These changes indicate a substantial reduction in crystallinity, yielding a predominantly amorphous product. The same trend is observed for both molar ratios, indicating that the preparation method has a major influence on the solid-state structural organization of the FEN–HP-β-CD systems. Among the investigated methods, lyophilization appears to be the most effective in forming a complexation compound.

The thermal properties of the pure compounds (FEN and HP-β-CD) and their physical mixtures and the products obtained using coprecipitation, lyophilization, and kNeading methods in 1:0.25 and 1:0.5 molar ratios were evaluated using thermal analysis. The TG/DTA curves are represented in Figure 4.

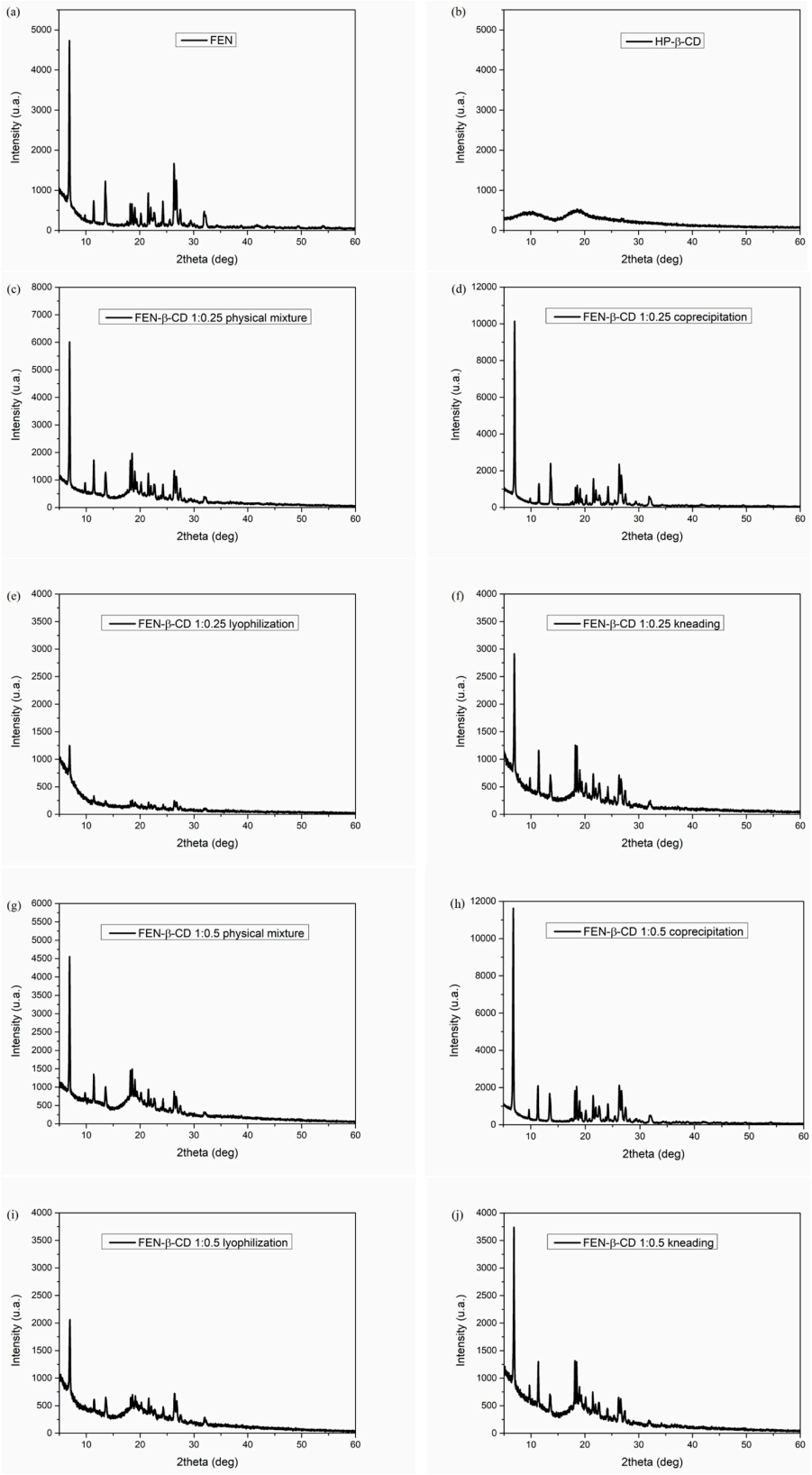


Figure 3. XRD analysis of (**a**) FEN; (**b**) HP-β-CD; (**c**) physical mixture between FEN and HP-β-CD in 1:0.25 molar ratio and its inclusion complexes; (**d**) FEN-HP-β-CD coprecipitation; (**e**) FEN-HP-β-CD lyophilization and (**f**) FEN-HP-β-CD kNeading; (**g**) physical mixture between FEN and HP-β-CD in 1:0.5 molar ratio and its inclusion complexes; (**h**) FEN-HP-β-CD coprecipitation; (**i**) FEN-HP-β-CD lyophilization and (**j**) FEN-HP-β-CD kNeading.

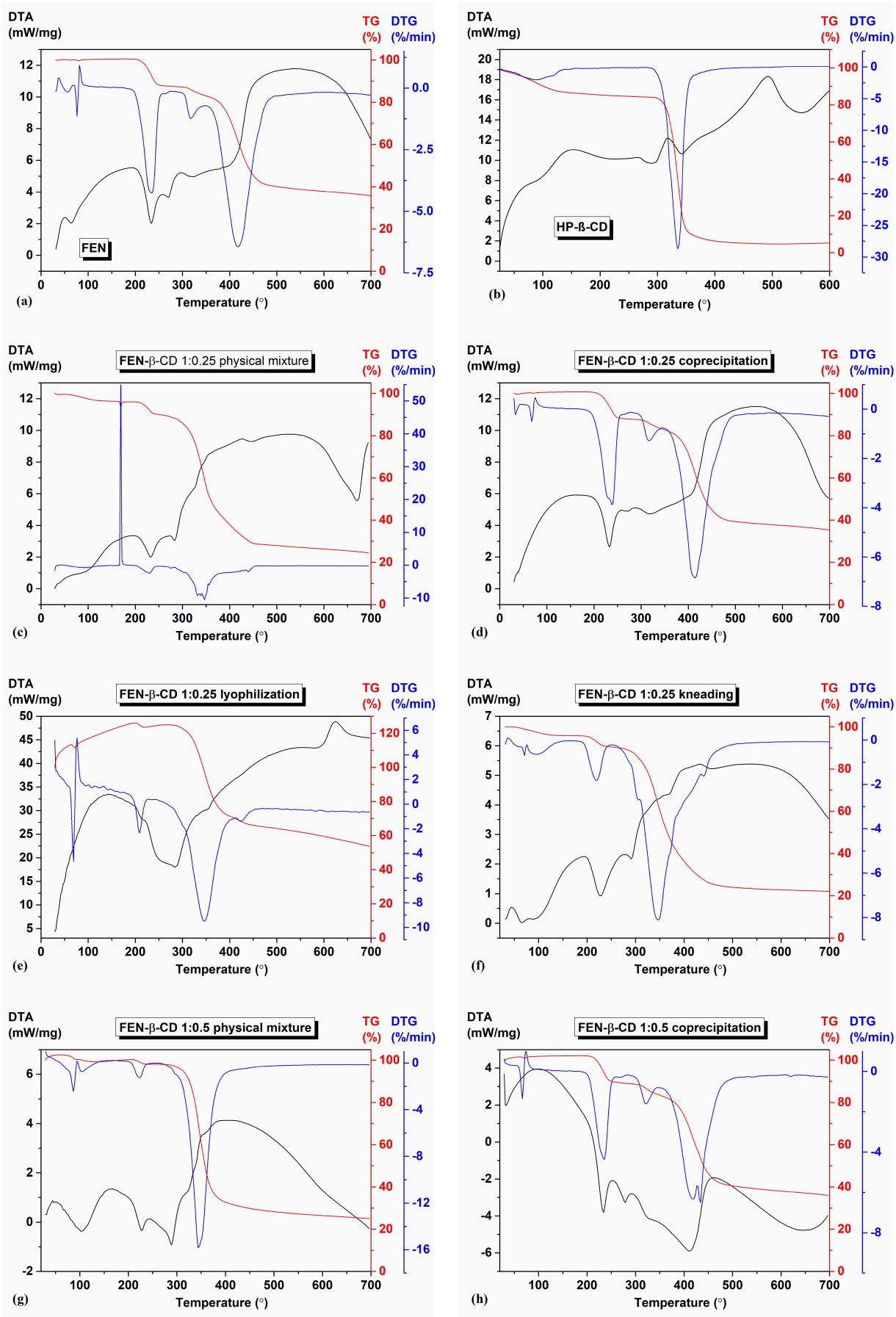


Figure 4. *Cont.*

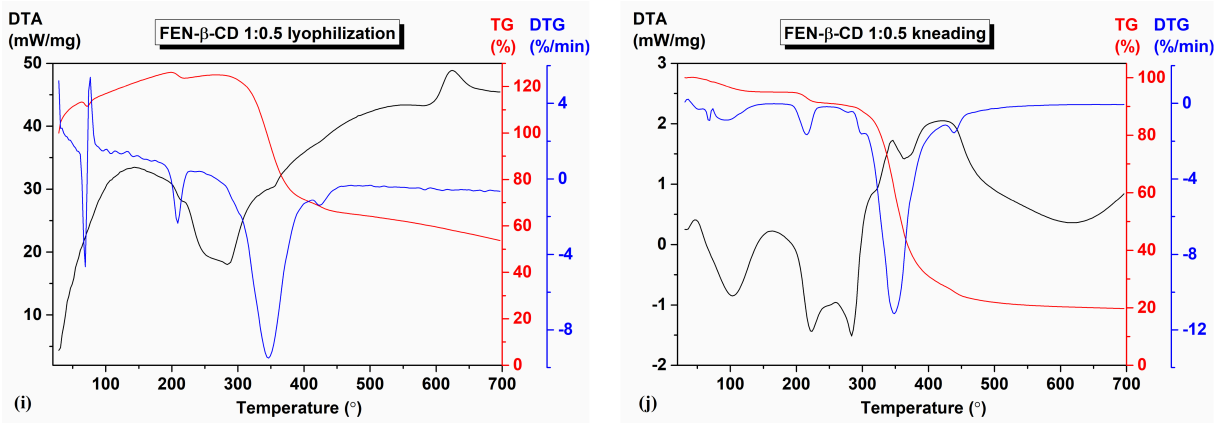


Figure 4. TG/DTA curves of (**a**) FEN; (**b**) HP-β-CD; (**c**) physical mixture between FEN and HP-β-CD in 1:0.25 molar ratio and its inclusion complexes; (**d**) FEN-HP-β-CD coprecipitation; (**e**) FEN-HP-β-CD lyophilization and (**f**) FEN-HP-β-CD kNeading; (**g**) physical mixture between FEN and HP-β-CD in 1:0.5 molar ratio and its inclusion complexes; (**h**) FEN-HP-β-CD coprecipitation; (**i**) FEN-HP-β-CD lyophilization and (**j**) FEN-HP-β-CD kNeading.

The TG/DTG curve of FEN (Figure 4a) showed that the FEN is stable under 200 °C followed by four main decomposition steps. The first step is from 200 to 261 °C with 12.3% mass loss, the second step is between 261 and 305 °C with 1.2% mass loss, the third step is between 305 and 381 °C with 7.3% mass loss, and the fourth step is between 381 and 500 °C with a mass loss of 41%. The residue at 700 °C is about 36%. The main decomposition process is due to the organic parts of the FEN and the residue and is attributed to the carbonaceous part, as mentioned in the literature [34,35]. The hydroxypropyl-β-cyclodextrin shows, initially, between 80–130 °C, a mass loss which corresponds to the loss of absorbed water molecules from the inside and outside of the cyclodextrin cavity (13.1% hydroxypropyl-β-cyclodextrin) (Figure 4b). The degradation process of HP-β-CD occurs between 300 and 400 °C with a residue at 700 °C of 4.7% [13].

Thermogravimetric and differential thermal analysis (TG/DTA) provided clear evidence of solid-state phase transformation (Figure 4). On the DTA curve of pure fenbendazole (Figure 4a), a sharp endothermic peak is observed at 233.5 °C (ΔH = 138.4 J/g), corresponding to the characteristic melting point of its crystalline form, followed by thermal decomposition above 260 °C. In the physical mixtures (Figure 4c,g), this endothermic melting peak remains detectable, indicating that simple physical blending does not alter the crystalline lattice of the drug. In contrast, in the binary systems prepared via lyophilization (Figure 4e,i), the endothermic melting peak of fenbendazole completely disappears for both the 1:0.25 and 1:0.5 molar ratios. The absence of this melting event demonstrates that the crystalline lattice of fenbendazole was effectively disrupted.

For the lyophilized products selected for tablet manufacturing, the sublimation process at −60 °C under high vacuum (<0.1 mbar) for 18 h effectively removed volatile organic residues, as corroborated by the absence of residual solvent mass loss below 100 °C in the TG/DTA curves.

While FTIR, XRD, and TG/DTA collectively demonstrate the loss of drug crystallinity, intimate molecular dispersion and extensive intermolecular interactions, they reflect solid-state amorphization rather than definitive structural proof of complete inclusion geometry. Therefore, the systems are more accurately described as amorphous drug–cyclodextrin solid complexes. The lyophilization method results in predominant amorphization of fenbendazole and the formation of a homogeneous amorphous matrix containing inclusion complexes, effectively overcoming the crystal lattice barrier of the drug for both evaluated molar ratios.

3.3. Characterization of the Powder Mixtures for Direct Compression

3.3.1. Particle Size Distribution

The granulometry of raw materials is a critical parameter in the die filling phase, directly affecting the flow properties of powders, as well as the consistency and structural integrity of final tablets produced by direct compression technology. To ensure the manufacture of tablets with optimal pharmacotechnical and biopharmaceutical attributes, it is essential to calibrate an ideal particle size distribution [36]. Therefore, the determination of the particle size distribution range is a mandatory preliminary step in precompression tests. The analyses were performed on the three direct compression blends in comparison to the contained active ingredients. Figure 5 shows the histogram for the powders under study, highlighting the particle size distribution profile based on specific granulometric classes.

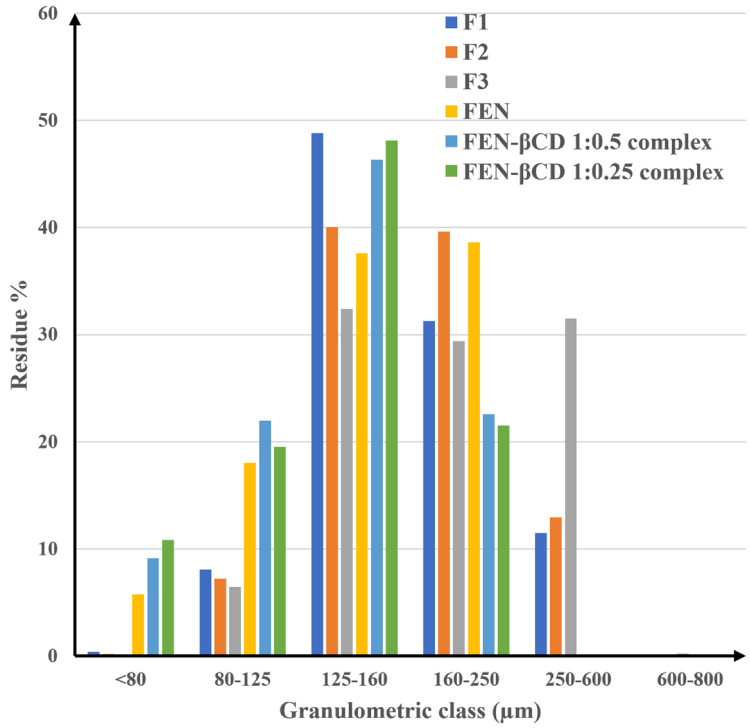


Figure 5. Particle size distribution.

Comparative analysis of the samples shows that most particles, regardless of material type, fall within the size range of 125 to 250 µm. According to Shekunov B.Y. et al. [37], a narrow particle size distribution gives powder systems superior rheological and compressibility properties, optimizing particle flow and rearrangement in tablets. Conversely, Wünsch et al. [38] demonstrated that compressibility tends to decrease in direct proportion to particle size reduction, a phenomenon attributed to the significant role of structural deformation mechanisms during dynamic compaction.

Among the active ingredients analyzed, although the differences are not highly pronounced, FEN alone shows a higher proportion of particles in the 160–250 µm size class compared to its inclusion complexes. This structural heterogeneity demonstrates the direct impact of HPβCD and the preparation method on the final particle size.

Quantitatively, the proportion of particles sized between 160 and 250 µm did not vary significantly in the inclusion complexes, being 22.56% for the FEN-HPβCD 1:0.5 system and 21.52% for the FEN-HPβCD 1:0.25 complex. It is also important to note that none of the binary systems investigated contained particle size fractions exceeding 250 µm.

Both inclusion compounds developed a higher volume fraction of particles in the 125–160 µm range, with minimal differences between the systems (46.33% for FEN-HPβCD 1:0.5 and 48.13% for FEN-HPβCD 1:0.25).

For powder mixtures for direct compression, the addition of excipients to the active systems significantly influences the geometric properties of the particles. In F1 to F3 formulations, there is a notable reconfiguration of the granulometric spectrum compared to FEN alone or its binary systems, characterized by a substantial increase in average particle size. Experimental analysis in these cases revealed the presence of a granulometric fraction with dimensions exceeding 250 µm.

However, differences between formulations are evident, as F3 containing FEN shows the highest proportion of particles in the 250–600 µm range (31.5%). In contrast, F1 and F2, based on FEN-HPβCD inclusion complexes, have a lower percentage of particles in the 250–600 µm range (11.49% for F1 and 12.93% for F2). As illustrated in the histogram (Figure 5), minor particle fractions smaller than 80 µm were detected (particularly for F1), along with a very small proportion of coarse particles in the 600–800 µm range for the final direct compression blends.

The influence of HPβCD is evident in both the binary systems and the direct compression powders. The data indicate that using HPβCD and the lyophilization technique results in a noticeable decrease in particle size, significantly impacting the overall mechanical behavior of the materials during compression.

Given these dimensional heterogeneities identified in the precompression phase, it can be reasonably anticipated that the developed materials will display distinct profiles and behaviors in terms of flowability and compressibility.

3.3.2. Moisture Content

Powder moisture is a critical parameter that directly affects both the final quality of the tablets and the homogeneity and behavior of the mixture during the compression process [39]. The measured moisture values for the samples are shown in Figure 6.

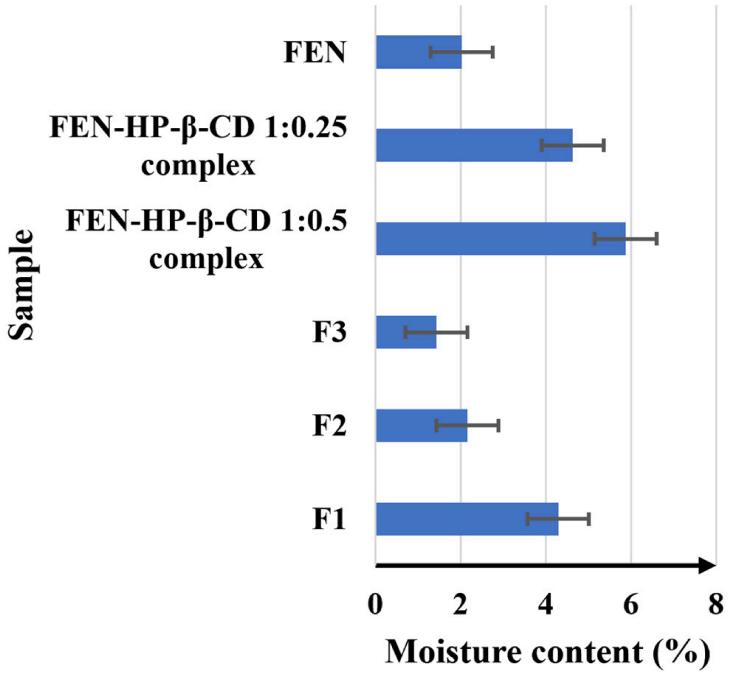


Figure 6. Moisture content of the analyzed materials.

Since the inclusion complexes were prepared in an aqueous phase before lyophilization, a certain amount of residual moisture in the final samples was expected. According to Koumbogle et al. [40], moisture mass transfer within the hygroscopic zone is mainly driven by vapor diffusion, as water vapor fills the internal pores and undergoes capillary condensation.

Elevated moisture levels generally increase both powder cohesion and flow energy [41], primarily because water content alters fundamental interparticulate forces, namely adhesion and friction [42]. Specifically, moisture deposited on particle surfaces can induce the formation of liquid bridges, enhancing capillary attraction and cohesive forces [43]. Consequently, this phenomenon may trigger powder agglomeration and a subsequent decline in flowability [44]. Conversely, a small fraction of water molecules can act as an internal lubricant, reducing friction and potentially optimizing flow properties [45]. Therefore, maintaining a low, well-controlled moisture threshold is vital, without exceeding critical limits. As reported by Crouter and Briens [46], moisture exerts a plasticizing effect on powder masses. Furthermore, Abu Fara et al. [47] demonstrated that complete dehydration can drastically impair the compressibility of solids, whereas excessive moisture tends to weaken interparticulate bonds, reducing the mechanical hardness of the resulting tablets. These established mechanisms provide a solid rationale for the compaction and flow behavior observed in our investigated materials.

While the two inclusion complexes showed only minor differences, a significant difference was observed between them and FEN alone. Notably, FEN had a very low moisture content (2.02%), in sharp contrast to its corresponding inclusion complexes, FEN-HP-β-CD 1:0.5 complex (5.87%) and FEN-HP-β-CD 1:0.25 complex (4.63%). This highlights the substantial impact of HP-β-CD on the structural configuration and resulting hygroscopic properties of the processed systems.

Additionally, a marked change in moisture levels was observed between the primary compounds and the direct compression blends. This decrease is directly attributed to the addition of tableting excipients, which significantly reduced the overall moisture content of the powder mass. The direct compression blends closely followed the trends of their respective primary systems, with formulation F3 showing the lowest residual moisture (1.43%), which was lower than the values for F1 (4.29%) or F2 (2.16%). These results demonstrate that the molar ratios of ingredients in the primary systems play a crucial role in determining the physical characteristics of the final materials.

3.3.3. Flowability

The results of the flow performance show a clear difference between the rheological behavior of the active ingredients and that of the compression mixtures.

None of the active ingredients (FEN and its two inclusion complexes in HP-β-CD) flowed, even when the samples were stirred at 25 rpm and the largest 25 mm nozzle was used. This demonstrates the strong cohesive character of the materials, which blocked the flow orifice even under forced dynamic conditions. This behavior is typical for systems obtained by lyophilization, a technological process that generates particles with increased porosity, low apparent density, and high surface energy. Electrostatic cohesion forces and Van der Waals interactions between the complex microparticles outweigh gravitational forces, making free flow difficult [11,48].

By contrast, all the direct compression powders exhibited free and continuous flow through the 25 mm nozzle without requiring mechanical stirring. This clear improvement in micromeritic properties validates the correct selection of the filler, microcrystalline cellulose, an agent recognized for its ability to optimize the flow and rheology of polydisperse systems [49].

As summarized in Table 3, the bulk density increased progressively from F1 (0.342 g/cm^3) to F3 (0.421 g/cm^3), inversely reflecting the proportion of the voluminous, low-density lyophilized complex. The dynamic angle of repose ranged from 29.8° (F3) to 34.2° (F1), remaining below the 35° threshold characteristic of satisfactory gravitational flow according to Ph. Eur. Correspondingly, flow time through the 25 mm nozzle varied from 14.5 s for F3 to 25.3 s for F1, confirming that all direct compression blends possess adequate flowability for high-speed tableting feed frames.

Table 3. Micromeritic and flowability parameters of the direct-compression powder blends (mean ± SD, $n = 3$).

Formulation	Bulk Density (g/cm^3)	Tapped Density (g/cm^3)	Hausner Ratio (HR)	Carr Index (CI, %)	Angle of Repose (°)	Flow Time (s)	Flow Rate (g/s, 25 mm nozzle)
F1	0.342 ± 0.012	0.455 ± 0.015	1.33 ± 0.02	24.86 ± 0.84	34.2 ± 1.1	25.3 ± 0.9	2.375 ± 0.082
F2	0.378 ± 0.011	0.492 ± 0.014	1.30 ± 0.02	23.19 ± 0.72	32.5 ± 0.9	20.00 ± 0.6	3.005 ± 0.091
F3	0.421 ± 0.015	0.515 ± 0.012	1.22 ± 0.01	18.22 ± 0.65	29.8 ± 0.8	14.5 ± 0.4	4.124 ± 0.115

The highest flow rate (4.124 g/s) was recorded for F3, which is not surprising given that it contains the highest amount of microcrystalline cellulose, the blend does not contain HP-β-CD, and the active ingredient was not lyophilized beforehand. The molecular weight and amorphous structure of the cyclodextrin increase the frictional forces between the particles, decreasing the overall flowability of the mixture [50].

Meanwhile, the lowest flow rate (2.375 g/s) was observed for F1, which contains the least microcrystalline cellulose and the highest proportion of HP-β-CD. F2 showed an intermediate value among the three materials, with a flow rate of 3.005 g/s.

The transition from a non-flowing profile of the active ingredients to mixtures with suitable flow rates for the direct compression process demonstrates the success of the preformulation phase. The developed blends ensure sufficient gravity flow to prevent segregation or misfeeding during compression, paving the way for stable and reproducible direct compression.

3.3.4. Volumetric Characteristics

The Carr index exceeded 40% for all three active ingredients, with the highest value observed for FEN (48.12%), followed by the FEN-HP-β-CD 1:0.5 lyophilized complex system (45.04%) and the FEN-HP-β-CD 1:0.25 lyophilized complex system (43.71%). The calculated Hausner ratios were above 1.70, indicating poor flowability and strong compressibility of the molecules. These results suggest significant interparticle cohesion.

A remarkable difference was observed for the direct compression powders, which showed Carr indexes below 25%, with the lowest value for F3 (18.22%). F3 contains FEN and the highest amount of microcrystalline cellulose, an excipient with excellent granular geometry, correlated with the use of FEN in its non-lyophilized state, which considerably reduces the surface energy of the powder system. The Carr index was 24.86% for F1 and 23.19% for F2. The HR values were 1.36 for F1, 1.30 for F2, and 1.23 for F3. This decreasing trend in compressibility indices from F1 to F3 demonstrates that reducing the proportion of HP-β-CD and increasing the microcrystalline cellulose fraction progressively improves the three-dimensional compaction of the particles, ensuring uniform die filling and reducing the risk of mass variation during the compression process [51].

Fluctuations in the flow properties of mixtures can cause major failures, such as non-uniform dosing unit mass, blockage of automated equipment, or segregation of active and auxiliary components. These phenomena directly affect the quality of finished products and compliance with regulatory standards. Irregular powder flow increases the risk of

weight variations and heterogeneous distribution of the active ingredient, which can lead to the rejection of production batches and limit process scalability at the industrial level. In key processes such as homogenization or direct compression, materials must pass through technological equipment without tendencies toward aggregation or interphase separation. Achieving optimal hardness and mass profiles during compression depends on the continuous and consistent feeding of the dies; any discontinuity caused by poor flowability can compromise the structural integrity of pharmaceutical forms through cracks or mechanical fractures. This highlights the need for a fundamental understanding of rheological characteristics to ensure process efficiency [52].

The functional properties of powders, such as compactability, flowability, and sensitivity to lubrication, are directly determined by their intrinsic attributes, including density and particle size distribution, with the preparation technology exerting considerable influence on particle structure [53].

The analysis of the studied systems confirms these interdependencies, highlighting a clear correlation between the rheological and compressibility behavior of the samples and their physical parameters, such as residual moisture, density, and particle size distribution. It has also been shown that the methodology used to obtain binary systems strongly influences the final physical properties of the materials. Systems obtained by lyophilization, characterized by higher water content and a prevalence of fine microparticles, exhibit significantly reduced flow capacity.

The overall physicomechanical properties of the final direct compression powders improve substantially. Furthermore, adding a minimal amount of magnesium stearate as a lubricant significantly optimizes the flowability of the powder mixtures without affecting the disintegration performance of the resulting tablets [54].

According to Li Z. et al. [55], the lyophilized powders show increased susceptibility to plastic deformation and superior compressibility, as the lyophilization process favors the formation of loose aggregates and highly porous three-dimensional networks during the solvent sublimation stage. A low bulk density indicates a pronounced densification tendency and is a direct consequence of increased internal porosity and imperfections in the network.

In this technological context, the beneficial effects of selected excipients on the flowability and compactability of systems are well documented, with the use of microcrystalline cellulose increasing the apparent density of powders [49]. The integration of this filler is particularly recommended for active ingredients with high water content, as it provides a matrix that ensures effective compressibility of the mixture and counteracts the negative effects of water on the mechanical properties and breaking strength of tablets [56]. Incorporating microcrystalline cellulose into systems with poor flowability results in a significant reduction in the Hausner ratio, Carr index, and angle of repose, due to decreased interparticle cohesion forces and optimized structural porosity of the material [57].

3.4. Tablets Quality Evaluation

From an organoleptic and morphological point of view, the tablets obtained are white, circular, smooth, free of asperities, and have a rigorously uniform macroscopic appearance.

The dimensional parameters of the tablets—thickness and diameter—as well as their individual mass, vary only within narrow limits, indicating uniform and reproducible filling of the compression matrices, directly determined by the suitable flow properties of the materials used. The compression process was carried out in full compliance with requirements due to the rigorous adjustment of all technological parameters of the equipment, as well as the adequate compactability of the formulation mixtures. The minor deviations recorded within the same batch or between different batches show that the type of active ingredient

used does not exert a significant influence on the mass or geometric dimensions of the resulting solid pharmaceutical forms. Tablet dimensions and mass properties showed tight reproducibility across all experimental series: average mass ($n = 20$) was 498.8 ± 4.2 mg for F1, 501.2 ± 3.8 mg for F2, and 499.5 ± 3.1 mg for F3, with individual deviations below 1.5% from theoretical weight (well within the ±5% compendial tolerance). Diameter was uniform at 13.02 ± 0.02 mm ($n = 10$), and tablet thickness ($n = 10$) was 4.18 ± 0.04 mm (F1), 4.21 ± 0.03 mm (F2), and 4.24 ± 0.03 mm (F3). These experimental data confirm the propriety of the selection of excipients and working conditions, demonstrating strict alignment with the quality criteria stipulated in the official monographs of the European Pharmacopoeia [17].

Ensuring strict compliance with uniform mass and dimensions is essential to guarantee an accurate therapeutic dose and optimal uniformity of active ingredient content in the final dosage units. According to the data reported by Hashmat D et al. [58], the physical characteristics of the powder systems, the dynamic fluctuations during feeding of the matrix filling segment, and the intensity of the applied compression force are determining factors for tablet weight constancy. Although the lyophilized intermediate powders exhibited low bulk density and cohesive behavior during preformulation screening, experimental quantification confirmed that the calibrated geometric blending process effectively prevented segregation during die filling. Assay and content uniformity testing demonstrated high dosing accuracy and uniformity: mean drug content was 99.2 ± 1.8% for F1, 98.6 ± 2.1% for F2, and 100.4 ± 1.5% for F3. All experimental batches met the compendial uniformity specification, yielding AV of 4.3 (F1), 5.2 (F2), and 3.6 (F3), all well below the maximum allowable threshold (AV ≤ 15.0). Moreover, no individual tablet fell outside the 85–115% dose range, confirming that the optimized proportions of microcrystalline cellulose and magnesium stearate provided sufficient blend cohesion and flow consistency to maintain content uniformity across all manufactured batches.

Correlating these aspects with our own experimental data, it can be deduced that all these critical variables were adequately monitored and controlled during the technological design phase, allowing us to obtain solid preparations that fully satisfy the imposed pharmacotechnical requirements.

Tablet hardness showed significant variation among the formulations, demonstrating the considerable influence of the presence and amount of HP-β-CD on the mechanical resistance of the tablets. Formulation F1 exhibited significantly higher mechanical hardness (98.2 ± 3.5 N) than F2 (87.4 ± 2.9 N, $p < 0.01$) and F3 (65.1 ± 2.4 N, $p < 0.001$; one-way ANOVA followed by Tukey's HSD test).

Tablet hardness is a critical parameter in pharmaceutical technology, directly reflecting the cohesion of the solid network formed during direct compression [59]. From a technological perspective, all three formulations (F1, F2, and F3) exhibit appropriate hardness values, ensuring adequate resistance during subsequent primary packaging and transport operations [60].

Traditionally, microcrystalline cellulose is regarded as a high-performing dry binder for direct compression due to its remarkable capacity for plastic deformation and hydrogen bond formation [61]. Surprisingly, although the amount of Avicel® pH 102 increases substantially from F1 (141 mg/tablet) to F3 (385 mg/tablet), tablet hardness decreases significantly.

Obtaining the inclusion complex by lyophilization radically modifies the solid state of the system, transforming the crystalline structure into a highly amorphous, porous, and stable matrix. Under compression, amorphous cyclodextrins exhibit a high degree of plastic deformation and controlled fragmentation. This destruction of micropores within the lyophilizate exponentially increases the effective contact surface between particles [62,63].

Furthermore, the HP-β-CD macromolecule presents a large number of free hydroxyl groups. At the moment of punch impact, these hydrophilic groups generate a dense, tight secondary network of interparticle hydrogen bonds, which acts as structural cement [64]. The fact that F1 reaches the maximum hardness value shows that the binding performance of cyclodextrin amorphized by lyophilization surpasses and enhances the effect of Avicel® pH 102. The molecular inclusion of FEN in the HP-β-CD cavity completely neutralizes the elastic behavior of the pure anthelmintic.

It is well established in solid-state pharmaceutics that mechanical compaction stress can occasionally induce phase transformations, potentially triggering pressure-induced recrystallization of metastable amorphous materials [65]. In the present formulations, applying a 30 kN compression force yielded compacts with high mechanical resistance (87–98 N). Critically, the in vitro dissolution profiles provide unambiguous functional evidence that the amorphous state was fully retained following tableting. If the mechanical energy of compaction had triggered nucleation or recrystallization of fenbendazole, the dissolution performance of tablets F1 and F2 would have deteriorated toward the plateau observed for the crystalline control tablets F3 (Q_{60}~63%). Instead, both cyclodextrin-based tablets preserved near-complete drug release at 60 min (96.8% for F1 and 99.5% for F2), with F1 displaying an immediate burst release of ~54% at 5 min. This retention of the amorphous state under high compaction force can be explained by two protective mechanisms: first, the high proportion of plastically deforming microcrystalline cellulose (Avicel® pH 102, 28–53%) buffers and dissipates localized mechanical shear during punch displacement; second, the bulky, steric architecture of the HP-β-CD matrix restricts molecular mobility during the millisecond compression dwell time, preventing crystal lattice rearrangement. While these functional release kinetics confirm that the amorphous advantage is maintained in the finished compacts, dedicated post-compaction PXRD and solid-state thermal profiling will be systematically incorporated into future ICH stability and scale-up studies to monitor physical integrity over extended shelf life.

The variation in hardness provides direct experimental evidence of the structural phase change. The proportion of HP-β-CD exerts strict, directly proportional control over mechanical strength: the greater the amount of lyophilized complex, the more compact, rigid, and stable the tablet's solid network becomes, representing a major technological advantage for the integrity of the final pharmaceutical form [66].

According to the European Pharmacopoeia, the acceptability and compliance criterion is strictly limited to a total mass loss of no more than 1.0% of the initial weight of tablets subjected to the friability test [17]. Friability testing ($n = 10$) yielded mass losses of 0.42 ± 0.05%$ for F1, 0.48 ± 0.06% for F2, and 0.65 ± 0.08% for F3. All formulations met the Ph. Eur. specification (mass loss ≤ 1.0%), with no capping, chipping, or tablet cleavage observed. The fact that all three experimental formulations recorded friability values below the 1% threshold demonstrates adequate peripheral structural integrity and optimal particle cohesion at the tablet surface [67].

This performance is due to the major role of microcrystalline cellulose. Avicel® pH 102 is an excipient with exceptional plastic properties; under compression, it undergoes permanent deformation that packs and tightly captures the active ingredients in a three-dimensional fibrous matrix. This peripheral network of microcrystalline cellulose gives the tablet controlled elasticity and remarkable surface strength, preventing capping or lamination even at more moderate overall hardness [68].

Another factor that explains the success of the friability test is the optimization of lubricant concentration. In pharmaceutical technology, magnesium stearate, although indispensable for reducing friction with punches, is kNown for its undesirable hydrophobic side effect: when used in excess or overmixed, it coats particles with an inert film that

prevents effective binding, reduces hardness, and dramatically increases friability. Maintaining magnesium stearate at an optimal concentration of 1% in all three formulations ensured adequate powder flow lubrication without interfering with the formation of solid interparticle bridges [69].

Friability values below 1% for all formulations confirm the appropriate selection of excipient types and quantities and the suitability of the direct compression process. The data demonstrate an optimal balance between hardness and surface elasticity, ensuring robust and mechanically stable FEN tablets.

Determining disintegration time is a critical performance parameter for solid, immediate-release pharmaceutical dosage forms. This test measures the time required for a tablet, under the action of a liquid medium and standardized mechanical agitation, to break down into agglomerated particles or fine granules. This is a mandatory preliminary and rate-limiting step for the subsequent dissolution of the active ingredient. According to the standards provided by the European Pharmacopoeia for uncoated tablets, the maximum allowed disintegration time is 15 min (900 s) [17].

The experimental results obtained for the three formulations show remarkably low values, well below the pharmacopoeial limit, which supports the selection and proportion of excipients used. Disintegration time was significantly shorter for F1 (58 ± 3.2 s) compared to F3 (77 ± 4.5 s, $p < 0.01$), despite the higher compact hardness of F1. F2 has an intermediate time at 69 ± 2.8 s.

In pharmaceutical technology, tablet hardness is directly proportional to disintegration time: a higher mechanical resistance implies denser compaction, reduced residual porosity, and consequently slower water penetration into the matrix, leading to slower disintegration [70].

Remarkably, the experimental data reveal an inverted behavior: formulation F1, although it showed the highest hardness (98 N), disaggregated the fastest (58 s). In contrast, formulation F3, with the lowest hardness (65 N), exhibited the slowest disintegration (77 s). This particularly interesting phenomenon can be explained by different physicochemical mechanisms.

Amorphous HP-β-CD obtained by lyophilization has a high thermodynamic affinity for water because of its dense peripheral hydroxyl groups. Its amorphous structure maintains a network of microscopic channels. When it contacts the test medium, even though the F1 tablet is highly compacted, the cyclodextrin functions as a hydrophilic wetting accelerator, rapidly drawing water into the solid core through advanced capillarity (wicking effect) [71,72]. The ultra-rapid dissolution of the amorphous cyclodextrin matrix leaves a highly porous structure, causing the tablet to lose its integrity almost instantly.

Pure FEN (used in the control formulation F3) is a highly hydrophobic substance (BCS class II/IV) with a surface energy that repels water. In the F3 formulation, crystalline FEN is freely dispersed in the Avicel® matrix. Although the F3 tablet has weaker cohesion (65 N) and, theoretically, larger interparticle spaces, the hydrophobic FEN crystals act as localized water-repellent barriers. They block the capillary channels of the microcrystalline cellulose and prevent effective water penetration [73,74]. As a result, water penetration is delayed, extending the disintegration time to 77 s.

All three formulations contain the same proportion of superdisintegrant (sodium starch glycolate, 2%). Its main mechanism of action is rapid and extensive swelling (an increase in particle volume of up to 300 times upon contact with water), which generates internal hydrostatic pressure that breaks the tablet from within. For this swelling mechanism to be efficiently triggered, the excipient requires a rapid influx of water [75]. In F1, the presence of the maximum amount of HP-β-CD delivers water to the Explotab® particles almost instantly, triggering explosive swelling and disintegration in just 58 s. In F3, due to

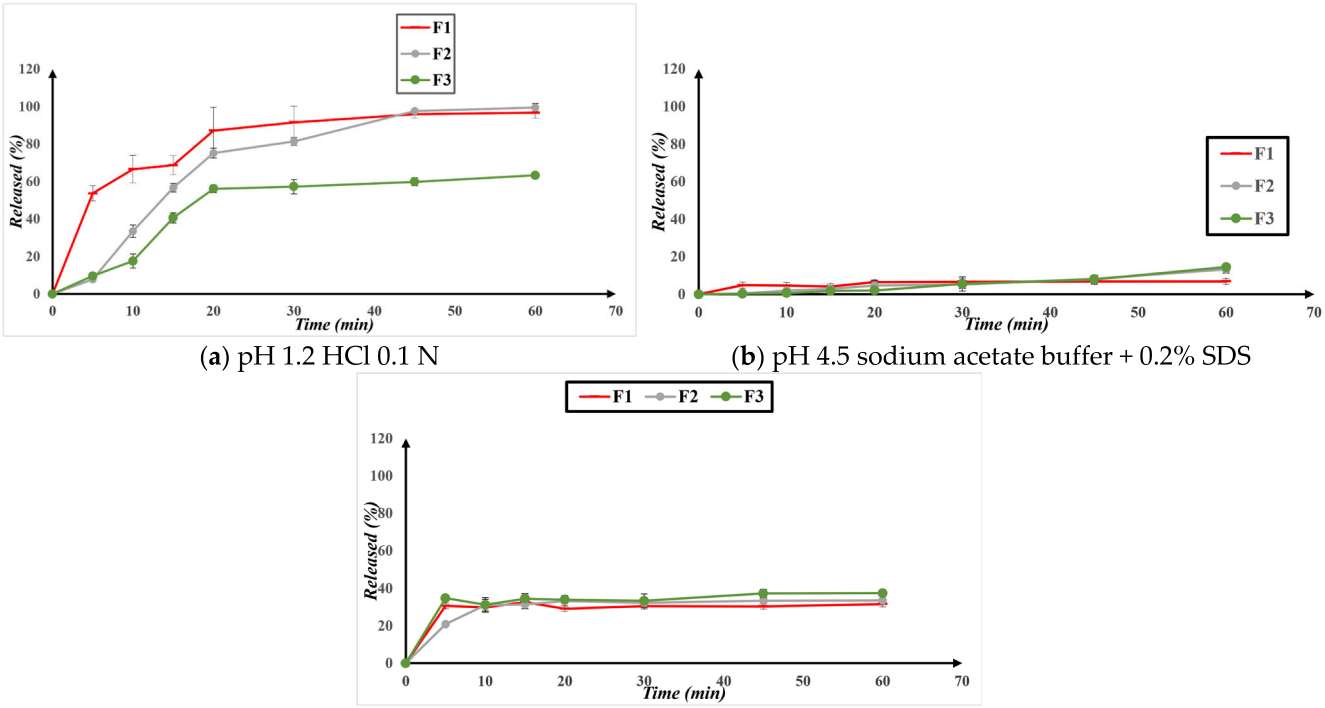
the hydrophobic shielding caused by pure FEN, Explotab® hydration is partially slowed, which explains the observed kinetic gap.

The variation in disintegration times confirms the strategic success of including FEN in the HP-β-CD complex. Modifying the solid state not only improves the mechanical properties but also completely eliminates the hydrophobic behavior of the active substance at the matrix level. This ultra-fast disintegration profile (under one minute for F1) represents an important technological premise, anticipating a superior dissolution rate.

Applying a 30 kN compression force ensured robust mechanical interlocking of the amorphous cyclodextrin particles, resulting in high hardness values (98 N for F1) without compromising ultra-fast disintegration, because the hydrophilic matrix and Explotab® facilitated rapid wicking that counterbalanced compact densification.

Evaluating the in vitro dissolution profile is the fundamental predictive test for the biological performance of an immediate-release solid dosage form, as it is directly correlated with the in vivo absorption process. For substances classified in BCS classes II and IV, such as FEN, increasing the rate and extent of dissolution is essential for improving their limited oral bioavailability [76].

Figure 7a–c shows the in vitro dissolution profiles of fenbendazole from the two cyclodextrin-based formulations (F1, F2) and from the uncomplexed drug (F3) in the three media. Because fenbendazole is a poorly water-soluble weak base, its dissolution behavior is strongly pH-dependent: solubility is relatively higher under acidic conditions and progressively lower as pH approaches neutrality. This intrinsic behavior governs the interpretation of the cyclodextrin effect in each medium and clarifies why the influence of HP-β-CD is not uniform across the pH range studied [5].



(**a**) pH 1.2 HCl 0.1 N

(**b**) pH 4.5 sodium acetate buffer + 0.2% SDS

(**c**) pH 6.8 phosphate buffer

Figure 7. In vitro dissolution profiles of fenbendazole from the test formulations (F1–F3): (**a**) pH 1.2 HCl 0.1 N; (**b**) pH 4.5 sodium acetate buffer; and (**c**) pH 6.8 phosphate buffer. Results are presented as mean ± SD ($n = 3$).

In the acidic medium (pH 1.2), F1 shows a superior kinetic profile, with a pronounced burst release in the first minutes of the test. After only 5 min, F1 has already released

~54% of the FEN dose. After 20 min, the percentage of dissolved active substance reaches ~87% for F1, satisfying the regulatory criteria established by FDA and EMA guidance for immediate-release oral solid dosage forms, which recommend that at least 85% of the labeled active substance should dissolve within 15 to 30 min. By the end of the interval (60 min), the curve reaches a higher plateau at ~97% (DE% = 81.8; MDT = 9.3 min).

At pH 1.2, both cyclodextrin formulations achieved significantly higher dissolution efficiency (81.8 ± 1.9% for F1 and 71.4 ± 2.3% for F2) compared with the uncomplexed drug formulation F3 (47.5 ± 1.7%, $p < 0.001$).

The superior wetting and hydration capacity provided by the FEN-HP-β-CD 1:0.5 inclusion complex of F1 determines not only rapid disintegration, but also instantaneous solubilization of FEN molecules in acidic medium.

F2 exhibits dissolution kinetics characterized by an initial lag phase followed by a pronounced acceleration. In the first 5–10 min, dissolution is slower than in F1, reaching only ~8% at minute 5 and ~33% at minute 10. This difference is attributed to the lower amount of hydrophilic agent, which requires additional time for complete hydration of the solid system [77]. Between minutes 10 and 20, F2 recovers substantially, reaching ~75% at minute 20 and ~81% at minute 30. Starting at minute 45, F2 matches and even slightly exceeds the F1 curve, achieving a practically complete release of ~100% at minute 60 (DE% = 71.4).

The behavior of the control batch F3 highlights the low solubility of FEN in its raw crystalline state. Although the F3 tablet disintegrated in 77 s due to the superdisintegrant Explotab®, this did not translate into efficient dissolution of the drug. At 10 min, the release is only ~18%. The F3 curve reaches a plateau (local saturation) relatively quickly, stabilizing at ~56% at 20 min and ~57% at 30 min. At the end of the test (60 min), F3 dissolves only ~63% of the dose (DE% = 47.5), with the rest of the active substance remaining as an insoluble crystalline suspension.

The clear difference between the dissolution profiles directly confirms the favorable modification of the solid state through inclusion in HP-β-CD.

In F3, the high energy of the crystal lattice of FEN, combined with its intrinsic hydrophobicity, prevents solvation of the molecules [9]. Once the tablet has disintegrated, the fine FEN particles float as agglomerates at the surface or bottom of the medium, without entering into solution [78].

The remarkable acceleration of dissolution observed for formulations F1 and F2 cannot be attributed solely to solid-state amorphization of the drug, but rather to a multifactorial mechanistic synergy. First, disruption of the crystalline lattice of fenbendazole during lyophilization eliminates the high lattice energy barrier (ΔH_{fusion}~138.4 J/g), facilitating rapid solvation. Second, the hydrophilic exterior of HP-β-CD, rich in peripheral hydroxyl groups, lowers the solid–liquid interfacial tension and acts as a steric wetting promoter that prevents particle agglomeration upon contact with the aqueous medium. Third, at the tablet matrix level, the hydrophilic cyclodextrin network accelerates capillary water uptake, rapidly delivering water to the embedded sodium starch glycolate particles; this triggers explosive volumetric swelling, breaking down the compact core within seconds (<70 s) and exposing a high effective surface area. Fourth, the acidic environment of 0.1 N HCl (pH 1.2) promotes protonation of the basic imidazole nitrogen (pKa~4.05), inducing chemical ionization. Together, the interplay of solid-state amorphization, localized wetting enhancement, ultrafast matrix disintegration, and pH-dependent ionization drives the near-instantaneous solubilization of fenbendazole from the F1 and F2 compacts [79]. The soluble complex dissolves as a whole, releasing the FEN molecules directly into solution, ready for absorption.

The dose-dependent effect of cyclodextrin is clearly visible in the first 20 min, during which F1 (ratio 1:0.5) overtakes F2 (ratio 1:0.25), confirming that a higher density of host molecules significantly improves the initial dissolution rate.

The choice of 0.1 N HCl (pH 1.2) as the dissolution medium is highly significant, as it simulates the physiological gastric environment and highlights the pH-dependent solubility profile of FEN. As a weak base, the benzimidazole ring undergoes partial protonation in strongly acidic media, leading to ionization and a subsequent increase in apparent solubility [80]. This chemical ionization explains why the control formulation (F3) reached a dissolution plateau of approximately 63% at 60 min.

However, despite the thermodynamic advantage provided by acidic protonation, dissolution of pure crystalline fenbendazole (F3) remained incomplete and was strongly limited by its high crystal lattice energy and hydrophobic surface. In stark contrast, formulations F1 and F2 successfully exploited a strong synergy between chemical protonation and matrix amorphization. Encapsulation of FEN within the highly hydrophilic HP-β-CD cavity, combined with its transition from a crystalline to an amorphous state via lyophilization, completely bypassed the initial wetting barrier. Consequently, ionized FEN molecules were released instantly into the medium as a soluble complex, allowing F1 to exhibit a burst effect (~54% in 5 min) and F2 to achieve complete dissolution (~100% at 60 min). This confirms that physical complexation with cyclodextrins is crucial, as acidic protonation alone is insufficient to guarantee complete dose dissolution for such high-melting-point, poorly water-soluble anthelmintics.

To evaluate the biopharmaceutical performance of the tablets in a physiological scenario simulating gastrointestinal transit or the postprandial state, dissolution profiles were monitored in sodium acetate buffer (pH 4.5) supplemented with 0.2% sodium dodecyl sulphate (SDS). The addition of the anionic surfactant SDS is a critical methodological requirement to maintain sink conditions for highly lipophilic substances (BCS Class II/IV), mimicking the natural surfactant action of bile acids and lecithin in intestinal fluids [81]. The results illustrated in Figure 7b highlight kinetic behavior different from that observed in a strongly acidic environment.

In the mildly acidic medium, drug release was minimal for all formulations (<15% at 60 min), reflecting the low solubility of fenbendazole at this pH even in the presence of a surfactant. F1 reached a low plateau of approximately 7% early, whereas F2 and F3 released the drug slowly but progressively, reaching 14.5 ± 0.9% and 13.3 ± 0.7% at the final time point, respectively (MDT ≈ 34–38 min versus 8.9 min for F1). Thus, release remained pharmaceutically negligible in this medium.

Interestingly, formulation F1, despite containing the highest proportion of HP-β-CD, exhibited the lowest cumulative release (~7%) in this medium. A plausible mechanistic hypothesis for this behavior involves competitive host–guest displacement between the anionic surfactant and fenbendazole. Sodium dodecyl sulfate possesses an aliphatic hydrocarbon chain with a remarkably high binding affinity for the hydrophobic cavity of β-cyclodextrin derivatives (K_a~10^3–10^4 M^{-1}) [82], which is several orders of magnitude higher than the apparent stability constant of fenbendazole (K_{st}~25.2 M^{-1}). Upon contact with the dissolution medium, SDS molecules can competitively displace FEN from the HP-β-CD cavities. Because unionized fenbendazole exhibits negligible intrinsic aqueous solubility at pH 4.5 (<1 µg/mL), the displaced drug molecules rapidly precipitate within the immediate tablet microenvironment, resulting in a low apparent release plateau. Furthermore, complexation between SDS and cyclodextrin depletes the pool of free surfactant unimers, thereby elevating the effective critical micelle concentration and diminishing the extent of micellar solubilization in the boundary layer. While this competitive displacement mechanism provides a consistent thermodynamic rationale, it remains an inferred hypoth-

esis that warrants future experimental validation via isothermal titration calorimetry or competitive solution NMR.

For a complete biopharmaceutical characterization of tablet behavior along the entire gastrointestinal tract, the release profiles were also evaluated in phosphate buffer at pH 6.8, a medium that simulates physiological conditions in the jejunum and ileum (small intestine). Unlike the previous test at pH 4.5, this medium was not supplemented with surfactant (SDS), with the aim of studying the intrinsic release of the systems in the absence of a micellar solubilizer.

At pH 6.8, all three curves fell below the 40% threshold and merged into a flat plateau as early as minute 5. From a technological perspective, this result is a classic demonstration of the thermodynamic limitations of BCS class II/IV substances under non-sink (saturation) conditions.

The results illustrated in Figure 7c highlight a drastic change in the release kinetics for all three formulations (F1, F2, and F3), with the profiles becoming practically indistinguishable and plateauing prematurely at very low values. F3 (the control) stabilizes around ~35–37%. Formulations F1 and F2 (with lyophilized complex) follow a similar trajectory, plateauing at ~30–33%.

All profiles rose quickly and plateaued within roughly 15 min (MDT ≈ 4.5–6.3 min), indicating that the medium rapidly approached saturation with respect to fenbendazole, thereby limiting further differentiation among the formulations.

FEN is a weak base with low intrinsic solubility in water. At pH 6.8, the medium is well above the pKa of the benzimidazole group, so more than 99% of FEN molecules are in the molecular, non-ionized form. This free form is hydrophobic, has unfavorable hydration energy, and tends to precipitate immediately from solution [33].

In pharmaceutical dissolution methodology, discriminatory release profiles require adequate sink conditions, conventionally defined as a medium volume sufficient to maintain drug concentration below 10–30% of its saturation solubility ($S \geq 3$) [83] (Table 4). In the present study, the experimental saturation solubility (C_s) of fenbendazole at 37 °C differed drastically across media: C_s~125.0 µg/mL at pH 1.2 (yielding a sink index $S = 1.13$), C_s~18.5 µg/mL in pH 4.5 acetate buffer + 0.2% SDS ($S = 0.17$), and C_s~0.12 µg/mL in surfactant-free pH 6.8 phosphate buffer ($S = 0.001$). At pH 1.2, protonation of the imidazole nitrogen (pKa~4.05) provides sufficient intrinsic solubility to support near-sink dissolution. In contrast, at pH 4.5 and pH 6.8, severe non-sink conditions prevail ($S < 1$). Specifically, in surfactant-free phosphate buffer at pH 6.8, where >99.8% of fenbendazole molecules exist in their uncharged, hydrophobic molecular state, 900 mL of medium can dissolve less than 0.11 mg of the drug. Consequently, initial matrix disintegration instantly exhausts the solubilization capacity of the medium within the first 5 min, leading to immediate thermodynamic saturation and producing identical, premature release plateaus (~30–37%) for all three formulations, regardless of cyclodextrin complexation.

In the absence of protonation (as was the case at pH 1.2), the saturation solubility of FEN in pure phosphate buffer is extremely low. In the first 5 min, the disintegration energy provided by Explotab® and the initial wetting release a small fraction of particles. This fraction instantly consumes the dissolving capacity of the 900 mL of medium, reaching the thermodynamic saturation limit. As a result, the dissolution process stops abruptly for all formulations, producing perfectly horizontal lines from minute 5 to minute 60.

To quantify the pairwise comparisons, the difference (f1) and similarity (f2) factors were calculated for each cyclodextrin formulation using the uncomplexed drug F3 as the reference (Table 5). At pH 1.2, both formulations were clearly dissimilar to the reference (f2 = 21.49 for F1 and 30.44 for F2), whereas at pH 6.8, both formulations were similar to the reference (f2 = 65.96 and 61.35; f1 < 15), reflecting the modest, convergent release in that

medium. At pH 4.5, the two metrics disagreed: f2 nominally indicated similarity (68.74 and 92.88), while f1 indicated a difference (72.40 and 16.32). This discordance is an artifact of the near-zero release regime, in which profiles appear numerically "similar" simply because all release values are very small; the f2 value is therefore not pharmaceutically informative in that medium.

Table 4. Model-independent dissolution parameters (DE%, MDT, and cumulative release at 60 min, Q_{60}) for each formulation in the three media (mean ± SD, $n = 3$).

Medium	Formulation	DE% (0–60 min)	MDT (min)	Q_{60} (%)
pH 1.2	F1	81.8 ± 1.9 [a]	9.3 ± 0.8 [a]	96.8 ± 2.1 [a]
	F2	71.4 ± 2.3 [b]	16.9 ± 1.1 [b]	99.5 ± 1.8 [a]
	F3	47.5 ± 1.7 [c]	15.0 ± 1.0 [b]	63.3 ± 2.4 [b]
pH 4.5	F1	5.9 ± 0.4 [a]	8.9 ± 0.7 [a]	6.9 ± 0.6 [a]
	F2	5.4 ± 0.5 [a]	37.5 ± 2.2 [b]	14.5 ± 0.9 [b]
	F3	5.9 ± 0.4 [a]	33.5 ± 1.9 [b]	13.3 ± 0.7 [b]
pH 6.8	F1	29.3 ± 1.1 [a]	4.5 ± 0.4 [a]	31.7 ± 1.2 [a]
	F2	30.3 ± 1.3 [a]	5.6 ± 0.5 [a]	33.5 ± 1.4 [a]
	F3	33.5 ± 1.2 [b]	6.3 ± 0.6 [a]	37.5 ± 1.5 [b]

Different superscript letters ([a], [b], [c]) within the same dissolution medium indicate statistically significant differences between formulations (one-way ANOVA followed by Tukey's post-hoc test, $p < 0.05$).

Table 5. Difference (f_1) and similarity (f_2) factors for the cyclodextrin formulations versus the uncomplexed drug (F3) as reference, in each medium.

Medium	Comparison	f1	f2	Interpretation
pH 1.2	F1 vs. F3	83.93	21.49	Dissimilar
pH 1.2	F2 vs. F3	49.51	30.44	Dissimilar
pH 4.5	F1 vs. F3	72.40	68.74	Non-informative *
pH 4.5	F2 vs. F3	16.32	92.88	Non-informative *
pH 6.8	F1 vs. F3	12.40	65.96	Similar
pH 6.8	F2 vs. F3	11.16	61.35	Similar

* Discordance between f1 and f2 arising from the very low absolute release (<15%), where similarity is not pharmaceutically meaningful.

Taken together, evaluating dissolution across these three physiologically relevant media provides a more complete picture of formulation behavior than any single medium. The influence of HP-β-CD on fenbendazole release was strongly medium-dependent, with the highest effectiveness under acidic conditions. In the intermediate pH 4.5 medium, release remained negligible for all systems, and the rapid saturation observed at pH 6.8 limited the extent to which the formulations could be differentiated.

Although solid-state characterization confirmed predominant amorphization of fenbendazole in the lyophilized binary systems, amorphous phases represent thermodynamically metastable states prone to recrystallization upon exposure to humidity or elevated temperatures. The low residual moisture content observed in the direct compression tablets (1.43–4.29%) and the tight matrix provided by microcrystalline cellulose help retard molecular mobility. Nevertheless, dedicated long-term physical stability studies under ICH conditions (25 °C/60% RH and 40 °C/75% RH) using XRD and DSC will be essential in future investigations to confirm that the amorphous network maintains its amorphous integrity and superior dissolution performance over the intended shelf life.

Also, the dissolution testing was conducted as a preliminary formulation screening phase and compendial release testing ($n \geq 6$) will be applied in future scale-up validation.

From a biopharmaceutical perspective, these in vitro dissolution findings provide critical insight into the expected in vivo transit behavior of the developed tablets. After oral administration under fasted conditions, the immediate-release tablets enter the stomach (pH 1.2–2.0), where the synergy between excipient wetting, rapid superdisintegrant wicking, and basic imidazole protonation triggers near-complete dissolution (~97–100% within 30–60 min for F1 and F2). This rapid gastric release generates a transiently supersaturated drug solution. As gastric chyme is propelled across the pylorus into the duodenum, however, the surrounding microenvironmental pH rises sharply toward 6.0–6.8. Given the unionized state and negligible intrinsic solubility of fenbendazole at neutral pH (<0.1 μg/mL), there is a substantial thermodynamic risk of drug precipitation within the intestinal lumen unless this metastable supersaturation is maintained. In a postprandial state, endogenous bile salt–phospholipid mixed micelles can provide micellar entrapment, retard precipitation, and facilitate duodenal permeation. Conversely, under fasted conditions, rapid intestinal transit across the narrow duodenal absorption window would be required before extensive precipitation occurs [84]. These mechanistic considerations indicate that although cyclodextrin-based direct compression tablets resolve the initial gastric dissolution bottleneck, future in vivo pharmacokinetic studies in both fasted and fed states are indispensable to establish whether this in vitro gastric advantage translates into sustained systemic exposure.

4. Conclusions

The present study demonstrated the technological feasibility of producing immediate-release tablets containing fenbendazole by utilizing sub-stoichiometric amorphous HP-β-CD complexes (1:0.25 and 1:0.5 molar ratios) prepared via lyophilization. Solid-state characterization (FTIR, XRD, and TG/DTA) confirmed that lyophilization effectively disrupts the crystalline lattice of fenbendazole, generating amorphous drug dispersions with enhanced wetting properties. Direct compression produced robust compacts that fulfilled pharmacopoeial quality attributes, displaying adequate crushing strength, friability below 0.7%, and rapid disintegration. The dissolution advantage provided by the amorphous HP-β-CD complexes is most pronounced in acidic gastric conditions (pH 1.2), whereas under intermediate (pH 4.5) and near-neutral (pH 6.8) conditions, release remains strictly solubility-limited in the absence of biorelevant solubilizers. This approach transforms the erratic dissolution profile of the active substance into an enhanced in vitro dissolution profile, providing a rational biopharmaceutical basis that may translate into improved in vivo oral absorption; however, in vivo pharmacokinetic validation remains essential. As a limitation, the findings reported herein represent an in vitro proof of concept, and long-term physical stability under ICH conditions, alongside in vivo pharmacokinetic trials, will be required to confirm translational therapeutic efficacy. Overall, coupling sub-stoichiometric cyclodextrin amorphization with optimized direct compression represents an efficient, reproducible strategy to overcome the erratic gastric dissolution profile of fenbendazole.

Author Contributions: Conceptualization, R.-D.P., E.A.O. and A.M.M.; methodology, E.A.O., A.M.M. and I.M.; validation, R.-D.P. and E.A.O.; formal analysis, R.-D.P., E.A.O., A.M.M., C.-M.T., C.Ș., V.-A.S., V.B., D.C.C., A.C.F. and I.M.; investigation, R.-D.P., E.A.O., A.M.M., C.-M.T., C.Ș., V.-A.S., V.B., D.C.C., A.C.F. and I.M.; resources, E.A.O.; data curation, E.A.O., I.M. and A.M.M.; writing—original draft preparation, E.A.O., I.M. and A.M.M.; writing—review and editing, E.A.O. and A.M.M.; visualization, E.A.O. and A.M.M.; supervision, E.A.O. and A.M.M.; project administration, E.A.O.; funding acquisition, E.A.O. All authors have read and agreed to the published version of the manuscript.

Funding: This research received no external funding.

Institutional Review Board Statement: Not applicable.

Informed Consent Statement: Not applicable.

Data Availability Statement: The original contributions presented in this study are included in the article. Further inquiries can be directed to the corresponding authors.

Conflicts of Interest: The authors declare no conflicts of interest.

References

1. Chiang, R.; Syed, A.; Wright, J.; Montgomery, B.; Srinivas, S. Fenbendazole enhancing anti-tumor effect: A case series. *Clin. Oncol. Case Rep.* **2021**, *4*, 1–4.
2. Song, B.; Park, E.Y.; Kim, K.J.; Ki, S.H. Repurposing of benzimidazole anthelmintic drugs as cancer therapeutics. *Cancers* **2022**, *14*, 4601. [CrossRef] [PubMed]
3. Karimi, A.; Bezerra, G.S.N.; Higginbotham, C.L.; Lyons, J.G. Evaluation of the Drug–Polymer Compatibility and Dissolution Behaviour of Fenbendazole–Soluplus® Solid Dispersions Prepared by Hot-Melt Extrusion. *Polymers* **2026**, *18*, 333. [CrossRef] [PubMed]
4. Anastasiya, I.; Varlamova, P.P.; Kotchetkov, I.A.; Arkhipov, S.S.; Khalikov, M.V.; Arisov, V.E.A. Pharmacokinetic profile, tissue residue depletion and anthelmintic efficacy of supramolecular fenbendazole. *Intern. J. Pharm.* **2021**, *607*, 120957. [CrossRef] [PubMed]
5. Karimi, A.; Barea, P.; Benito-Román, Ó.; Blanco, B.; Sanz, M.T.; Higginbotham, C.L.; Lyons, J.G. Investigation of Fenbendazole Solubility Using Particle Size Reduction Methods in the Presence of Soluplus®. *Pharmaceutics* **2025**, *17*, 1163. [CrossRef] [PubMed]
6. Bezerra, G.S.N.; De Lima, G.G.; Colbert, D.M.; Halligan, E.; Geever, J.; Geever, L. Micro-Injection Moulding of PEO/PCL Blend–Based Matrices for Extended Oral Delivery of Fenbendazole. *Pharmaceutics* **2023**, *15*, 900. [CrossRef] [PubMed]
7. Esteso, M.A.; Romero, C.M. Cyclodextrins: Properties and Applications. *Int. J. Mol. Sci.* **2024**, *25*, 4547. [CrossRef] [PubMed]
8. Zheng, A.Y.; Heng, P.W.S.; Chan, L.W. Tablet Disintegratability: Sensitivity of Superdisintegrants to Temperature and Compaction Pressure. *Pharmaceutics* **2022**, *14*, 2725. [CrossRef] [PubMed]
9. Ding, Y.; Zhang, Z.; Ding, C.; Xu, S.; Xu, Z. Preparation and evaluation of fenbendazole methyl-β-cyclodextrin inclusion complexes. *BMC Vet. Res.* **2024**, *20*, 214. [CrossRef] [PubMed]
10. Vargas Michelena, L.; Bedogni, G.R.; Barraza, G.A.; Lamas, M.C.; Sanchez, A.M.; Salomon, C.J. Integrating NMR spectroscopy, molecular docking, and molecular dynamics simulations to elucidate fenbendazole–cyclodextrin complexation and its pH-dependent behavior. *J. Mol. Liq.* **2026**, *463*, 129960. [CrossRef]
11. Novac, M.; Musuc, A.M.; Ozon, E.A.; Sarbu, I.; Mitu, M.A.; Rusu, A.; Petrescu, S.; Atkinson, I.; Gheorghe, D.; Lupuliasa, D. Design and Evaluation of Orally Dispersible Tablets Containing Amlodipine Inclusion Complexes in Hydroxypropyl-β-cyclodextrin and Methyl-β-cyclodextrin. *Materials* **2022**, *15*, 5217. [CrossRef] [PubMed]
12. Mitu, M.A.; Cretu, E.A.; Novac, M.; Karampelas, O.; Nicoara, A.; Nitulescu, G.; Lupuleasa, D. The Flowing Characteristics of Some Composed Powders Containing Inclusion Complexes in Beta-Cyclodextrin. In *Proceedings of the 17th Romanian National Congress of Pharmacy, 17th Edition: 21st Century Pharmacy—Between Intelligent Specialization and Social Responsibility 2018 Bucharest, Romania, 26–29 September 2018*; Draganescu, D., Arsene, A., Eds.; InFOROmatica S.r.l.: Bologna, Italy, 2018; pp. 129–133.
13. Solomon, C.; Anuța, V.; Sarbu, I.; Ozon, E.A.; Musuc, A.M.; Bratan, V.; Rusu, A.; Surdu, V.-A.; Croitoru, C.; Chandak, A.; et al. Enhancing the Drug Release and Physicochemical Properties of Rivaroxaban via Cyclodextrin Complexation: A Comprehensive Analytical Approach. *Pharmaceuticals* **2025**, *18*, 761. [CrossRef] [PubMed]
14. Novac, M.; Musuc, A.M.; Ozon, E.A.; Sarbu, I.; Mitu, M.A.; Rusu, A.; Gheorghe, D.; Petrescu, S.; Atkinson, I.; Lupuliasa, D. Manufacturing and Assessing the New Orally Disintegrating Tablets, Containing Nimodipine-hydroxypropyl-β-cyclodextrin and Nimodipine-methyl-β-cyclodextrin Inclusion Complexes. *Molecules* **2022**, *27*, 2012. [CrossRef] [PubMed]
15. Putra, O.N.; Musfiroh, I.; Elisa, S.; Musa, M.; Ikram, E.H.K.; Chaidir, C.; Muchtaridi, M. Sodium Starch Glycolate (SSG) from Sago Starch (*Metroxylon sago*) as a Superdisintegrant: Synthesis and Characterization. *Molecules* **2023**, *29*, 151. [CrossRef] [PubMed]
16. Moreton, C. Functionality and performance of excipients in a quality-by design world, part VIII: Excipient specifications. *Am. Pharm. Rev.* **2010**, *13*, 46–50.
17. Council of Europe. *European Pharmacopoeia*, 10th ed.; EDQM, Council of Europe: Strasbourg, France, 2019.
18. Khan, K.A. The concept of dissolution efficiency. *J. Pharm. Pharmacol.* **1975**, *27*, 48–49. [CrossRef] [PubMed]
19. Mockel, J.E.; Lippold, B.C. Zero order release from hydrocolloid matrices. *Pharm. Res.* **1993**, *10*, 1066–1070. [CrossRef] [PubMed]
20. Food and Drug Administration (FDA). Dissolution Testing of Immediate Release Solid Oral Dosage Forms. 1997. Available online: https://www.fda.gov/regulatory-information/search-fda-guidance-documents/dissolution-testing-immediate-release-solid-oral-dosage-forms (accessed on 2 October 2026).
21. European Medicines Agency (EMEA). Guideline On The Investigation of Bioequivalence Discussion in the Joint Efficacy and Quality Working Group. 2010. Available online: http://www.ema.europa.eu (accessed on 2 October 2026).

22. Higuchi, T.; Connors, K.A. Phase solubility diagram. *Adv. Anal. Chem. Instr.* **1965**, *4*, 117–212. [CrossRef]
23. Hirlekar, R.S.; Sonawane, S.N.; Kadam, V.J. Studies on the effect of water-soluble polymers on drug-cyclodextrin complex solubility. *AAPS PharmSciTech* **2009**, *10*, 858–863. [CrossRef] [PubMed]
24. Budura, E.; Lupuleasa, D.; Aramă, C.; Nitulescu, M.; Balaci, T. Preparation and characterization of inclusion complexes formed between simvastatin and hydroxypropyl-β-cyclodextrin. *Farmacia* **2011**, *59*, 512–530.
25. Mason, R.P.; Rhodes, D.G.; Herbette, L.G. Reevaluating equilibrium and kinetic binding parameters for lipophilic drugs based on a structural model for drug interaction with biological membranes. *J. Med. Chem.* **1991**, *34*, 869–877. [CrossRef] [PubMed]
26. Weidner, T.; Breen, N.F.; Drobny, G.P.; Castner, D.G. Amide or Amine: Determining the Origin of the 3300 cm^{-1} NH Mode in Protein SFG Spectra Using 15 N Isotope Labels. *J. Phys. Chem. B* **2009**, *113*, 15423–15426. [CrossRef] [PubMed]
27. Takei, K.; Takahashi, R.; Noguchi, T. Correlation between the Hydrogen-Bond Structures and the C=O Stretching Frequencies of Carboxylic Acids as Studied by Density Functional Theory Calculations: Theoretical Basis for Interpretation of Infrared Bands of Carboxylic Groups in Proteins. *J. Phys. Chem. B* **2008**, *112*, 6725–6731. [CrossRef] [PubMed]
28. Mary, Y.S.; Jojo, P.J.; Panicker, C.Y.; Van Alsenoy, C.; Ataei, S.; Yildiz, I. Quantum Mechanical and Spectroscopic (FT-IR, FT-Raman, 1H NMR and UV) Investigations of 2-(Phenoxymethyl)Benzimidazole. *Spectrochim. Acta A Mol. Biomol. Spectrosc.* **2014**, *125*, 12–24. [CrossRef] [PubMed]
29. Yuan, C.; Liu, B.; Liu, H. Characterization of hydroxypropyl-β-cyclodextrins with different substitution patterns via FTIR, GC–MS, and TG–DTA. *Carbohyr. Polym.* **2015**, *118*, 36–40. [CrossRef] [PubMed]
30. Mrozek, M.F.; Weaver, M.J. Detection and identification of aqueous saccharides by using surface-enhanced Raman spectroscopy. *Anal. Chem.* **2002**, *74*, 4069–4075. [CrossRef] [PubMed]
31. Ozon, E.A.; Novac, M.; Gheorghe, D.; Musuc, A.M.; Mitu, M.A.; Sarbu, I.; Anuta, V.; Rusu, A.; Petrescu, S.; Atkinson, I.; et al. Formation and Physico-Chemical Evaluation of Nifedipine-hydroxypropyl-β-cyclodextrin and Nifedipine-methyl-β-cyclodextrin: The Development of Orodispersible Tablets. *Pharmaceuticals* **2022**, *15*, 993. [CrossRef] [PubMed]
32. Melian, M.E.; Munguía, A.B.; Faccio, R.; Palma, S.; Domínguez, L. The Impact of Solid Dispersion on Formulation, Using Confocal Micro Raman Spectroscopy as Tool to Probe Distribution of Components. *J. Pharm. Innov.* **2018**, *13*, 58–68. [CrossRef]
33. Bezerra, G.S.N.; de Lima, T.A.M.; Colbert, D.M.; Geever, J.; Geever, L. Formulation and Evaluation of Fenbendazole Extended-Release Extrudes Processed by Hot-Melt Extrusion. *Polymers* **2022**, *14*, 4188. [CrossRef] [PubMed]
34. Bezerra, G.S.N.; Moritz, V.F.; de Lima, T.A.D.M.; Colbert, D.M.; Geever, J.; Geever, L. Compatibility Study between Fenbendazole and Polymeric Excipients Used in Pharmaceutical Dosage Forms Using Thermal and Non-Thermal Analytical Techniques. *Analytica* **2022**, *3*, 448–461. [CrossRef]
35. Attia, A.K.; Saad, A.S.; Alaraki, M.S.; Elzanfaly, E.S. Study of thermal analysis behavior of fenbendazole and rafoxanide. *Adv. Pharm. Bull.* **2017**, *7*, 329–334. [CrossRef] [PubMed]
36. Kudo, Y.; Yasuda, M.; Matsusaka, S. Effect of particle size distribution on flowability of granulated lactose. *Adv. Powder Technol.* **2020**, *31*, 121–127. [CrossRef]
37. Shekunov, B.Y.; Chattopadhyay, P.; Tong, H.H.Y.; Chow, A.H.L. Particle Size Analysis in Pharmaceutics: Principles, Methods and Applications. *Pharm. Res.* **2006**, *24*, 203–227. [CrossRef] [PubMed]
38. Wünsch, I.; Finke, J.H.; John, E.; Juhnke, M.; Kwade, A. The influence of particle size on the application of compression and compaction models for tableting. *Int. J. Pharm.* **2021**, *599*, 120424. [CrossRef] [PubMed]
39. Wang, Y.; Li, T.; Muzzio, F.J.; Glasser, B.J. Predicting feeder performance based on material flow properties. *Powder Technol.* **2017**, *308*, 135–148. [CrossRef]
40. Koumbogle, K.; Gosselin, R.; Gitzhofer, F.; Abatzoglou, N. Moisture Behavior of Pharmaceutical Powder during the Tableting Process. *Pharmaceutics* **2023**, *15*, 1652. [CrossRef] [PubMed]
41. Juarez-Enriquez, E.; Olivas, G.I.; Zamudio-Flores, P.B.; Ortega-Rivas, E.; Perez-Vega, S.; Sepulveda, D.R. Effect of water content on the flowability of hygroscopic powders. *J. Food Eng.* **2017**, *205*, 12–17. [CrossRef]
42. Hirschberg, C.; Sun, C.C.; Risbo, J.; Rantanen, J. Effects of Water on Powder Flowability of Diverse Powders Assessed by Complimentary Techniques. *J. Pharm. Sci.* **2019**, *108*, 2613–2620. [CrossRef] [PubMed]
43. Mukherjee, R.; Sen, K.; Fontana, L.; Mao, C.; Chaudhuri, B. Quantification of Moisture-Induced Cohesion in Pharmaceutical Mixtures. *J. Pharm. Sci.* **2019**, *108*, 223–233. [CrossRef] [PubMed]
44. Lüddecke, A.; Pannitz, O.; Zetzener, H.; Sehrt, J.T.; Kwade, A. Powder properties and flowability measurements of tailored nanocomposites for powder bed fusion applications. *Mater. Des.* **2021**, *202*, 109536. [CrossRef]
45. Wu, Z.; Wu, Y.; Zakhvatayeva, A.; Wang, X.; Liu, Z.; Yang, M.; Zheng, Q.; Wu, C.Y. Influence of moisture content on die filling of pharmaceutical powders. *J. Drug Deliv. Sci. Technol.* **2022**, *78*, 103985. [CrossRef]
46. Crouter, A.; Briens, L. The effect of moisture on the flowability of pharmaceutical excipients. *AAPS PharmSciTech* **2014**, *15*, 65–74. [CrossRef] [PubMed]
47. Abu Fara, D.; Al-Hmoud, L.; Rashid, I.; Chowdhry, B.Z.; Badwan, A. Understanding the Performance of a Novel Direct Compression Excipient Comprising Roller Compacted Chitin. *Mar. Drugs* **2020**, *18*, 115. [CrossRef] [PubMed]

48. Blanco, D.; Antikainen, O.; Räikkönen, H.; Yliruusi, J.; Juppo, A.M. Effect of colloidal silicon dioxide and moisture on powder flow properties: Predicting in-process performance using image-based analysis. *Int. J. Pharm.* **2021**, *597*, 120344. [CrossRef] [PubMed]
49. Thoorens, G.; Krier, F.; Leclercq, B.; Carlin, B.; Evrard, B. Microcrystalline cellulose, a direct compression binder in a quality by design environment—A review. *Int. J. Pharm.* **2014**, *473*, 64–72. [CrossRef] [PubMed]
50. Volkova, T.V.; Simonova, O.R.; Perlovich, G.L. Cyclodextrin effects on the distribution, solubility and transport properties of umifenovir. *Colloids Surf. A Physicochem. Eng. Asp.* **2025**, *705*, 135574. [CrossRef]
51. Kirchengast, M.; Celikovic, S.; Rehrl, J.; Sacher, S.; Kruisz, J.; Khinast, J.G.; Horn, M. Ensuring tablet quality via model-based control of a continuous direct compaction process. *Int. J. Pharm.* **2019**, *567*, 118457. [CrossRef] [PubMed]
52. Beccaro, L.; Facco, P.; Dhenge, R.M.; Khala, M.J.; Cenci, F.; Bezzo, F.; Barolo, M. Accelerating pharmaceutical tablet development by transfer of powder compaction equipment across types and scales. *Int. J. Pharm.* **2024**, *667*, 124904. [CrossRef] [PubMed]
53. Chen, F.C.; Liu, W.J.; Zhu, W.F.; Yang, L.Y.; Zhang, J.W.; Feng, Y.; ming, L.S.; Li, Z. Surface Modifiers on Composite Particles for Direct Compaction. *Pharmaceutics* **2022**, *14*, 2217. [CrossRef] [PubMed]
54. Qu, L.; Zhou, Q.; Gengenbach, T.; Denman, J.A.; Stewart, P.J.; Hapgood, K.P.; Gamlen, M.; Morton, D.A.V. Investigation of the potential for direct compaction of a fine ibuprofen powder dry-coated with magnesium stearate. *Drug Dev. Ind. Pharm.* **2015**, *41*, 825–837. [CrossRef] [PubMed]
55. Li, Z.; Zhao, L.; Lin, X.; Shen, L.; Feng, Y. Direct compaction: An update of materials, trouble-shooting, and application. *Int. J. Pharm.* **2017**, *529*, 543–556. [CrossRef] [PubMed]
56. Olorunsola, E.O.; Akpan, G.A.; Adikwu, M.U. Evaluation of Chitosan-Microcrystalline Cellulose Blends as Direct Compression Excipients. *J. Drug Deliv.* **2017**, *2017*, 1–8. [CrossRef] [PubMed]
57. Chitedze, J.; Monjerezi, M.; Saka, J.D.K.; Steenkamp, J. Binding effect of cassava starches on the compression and mechanical properties of ibuprofen tablets. *J. App. Pharm. Sci.* **2012**, *2*, 31–37. [CrossRef]
58. Hashmat, D.; Shoaib, M.H.; Mehmood, Z.A.; Bushra, R.; Yousuf, R.I.; Lakhani, F. Development of Enteric Coated Flurbiprofen Tablets using Opadry/acryleze System—A Technical Note. *AAPS PharmSciTech* **2008**, *9*, 116–121. [CrossRef] [PubMed]
59. Mathe, R.; Casian, T.; Tomuta, I. Multivariate Data Analysis to Assess Process Evolution and Systematic Root Causes Investigation in Tablet Manufacturing at an Industrial Scale—A Case Study Focused on Improving Tablet Hardness. *Pharmaceutics* **2025**, *17*, 213. [CrossRef] [PubMed]
60. De Simone, V.; Caccavo, D.; Lamberti, G.; D'Amore, M.; Barba, A.A. Wet-granulation process: Phenomenological analysis and process parameters optimization. *Powder Technol.* **2018**, *340*, 411–419. [CrossRef]
61. Cabiscol, R.; Finke, J.H.; Zetzener, H.; Kwade, A. Characterization of Mechanical Property Distributions on Tablet Surfaces. *Pharmaceutics* **2018**, *10*, 184. [CrossRef] [PubMed]
62. Liew, K.B.; Peh, K.K. Investigation on the effect of polymer and starch on the tablet properties of lyophilized orally disintegrating tablet. *Arch. Pharm. Res.* **2021**, *44*, 1–10. [CrossRef]
63. Aldawsari, H.M.; Badr-Eldin, S.M. Enhanced pharmacokinetic performance of dapoxetine hydrochloride via the formulation of instantly-dissolving buccal films with acidic pH modifier and hydrophilic cyclodextrin: Factorial analysis, in vitro and in vivo assessment. *J. Adv. Res.* **2020**, *24*, 281–290. [CrossRef] [PubMed]
64. Alghaith, A.F.; Mahrous, G.M.; Zidan, D.E.; Alhakamy, N.A.; Alamoudi, A.J.; Radwan, A.A. Preparation, characterization, dissolution, and permeation of flibanserin—2-HP-β-cyclodextrin inclusion complexes. *Saudi Pharm. J.* **2021**, *29*, 963–975. [CrossRef]
65. Iyer, J.; Brunsteiner, M.; Modhave, D.; Paudel, A. Role of Crystal Disorder and Mechanoactivation in Solid-State Stability of Pharmaceuticals. *J. Pharm. Sci.* **2023**, *112*, 1539–1565. [CrossRef] [PubMed]
66. Raju Sagiraju, S.R.K.; Ekmekci, E.; Erol Aldeniz, E.; Dude, U.; Cagri, B. The effect of compaction force on tablet hardness and dissolution rate of a poorly soluble, BCS Class II, micronized API in lactose-based immediate release formulations: A case study with RSM historical data review using Design of Experiment. *Int. J. Pharm. Sci.* **2024**, *2*, 776–786. [CrossRef]
67. Zhao, H.; Yu, Y.; Ni, N.; Zhao, L.; Lin, X.; Wang, Y.; Du, R.; Shen, L. A new parameter for characterization of tablet friability based on a systematical study of five excipients. *Int. J. Pharm.* **2022**, *611*, 121339. [CrossRef] [PubMed]
68. Poudel, J.; Bhattarai, S.; Nath, N.; Tanti, B. An exclusive review of microcrystalline cellulose: Structure and applications, and limitations. *Mater. Today Commun.* **2025**, *45*, 112247. [CrossRef]
69. Uzunović, A.; Vranić, E. Effect of magnesium stearate concentration on dissolution properties of ranitidine hydrochloride coated tablets. *Bosn. J. Basic Med. Sci.* **2007**, *7*, 279–283. [CrossRef] [PubMed]
70. Markl, D.; Zeitler, J.A. A Review of Disintegration Mechanisms and Measurement Techniques. *Pharm. Res.* **2017**, *34*, 890–917. [CrossRef] [PubMed]
71. Demirturk, E.; Gundogdu, G.; Cetin, M.; Bilensoy, E. Improved Bioavailability of Spironolactone–Hydroxypropyl-β-Cyclodextrin Complex Tablets Evaluated in Rat Model. *J. Pharm. Innov.* **2026**, *21*, 541. [CrossRef]
72. Woldum, H.S.; Larsen, K.L.; Madsen, F. Cyclodextrin Controlled Release of Poorly Water-Soluble Drugs from Hydrogels. *Drug Deliv.* **2008**, *15*, 69–80. [CrossRef] [PubMed]

73. Berg, C.F. Permeability description by characteristic length, tortuosity, constriction and porosity. *Transp. Porous Media* **2014**, *103*, 381–400. [CrossRef]
74. Bawuah, P.; Pierotic Mendia, A.; Silfsten, P.; Pääkkönen, P.; Ervasti, T.; Ketolainen, J.; Zeitler, J.A.; Peiponen, K.-E. Detection of porosity of pharmaceutical compacts by terahertz radiation transmission and light reflection measurement techniques. *Int. J. Pharm.* **2014**, *465*, 70–76. [CrossRef] [PubMed]
75. Steffens, K.E.; Wagner, K.G. Immediate-Release Formulations Produced via Twin-Screw Melt Granulation: Systematic Evaluation of the Addition of Disintegrants. *AAPS PharmSciTech* **2021**, *22*, 183. [CrossRef]
76. Bhalani, D.V.; Nutan, B.; Kumar, A.; Singh Chandel, A.K. Bioavailability Enhancement Techniques for Poorly Aqueous Soluble Drugs and Therapeutics. *Biomedicines* **2022**, *10*, 2055. [CrossRef] [PubMed]
77. Karoyo, A.H.; Wilson, L.D. A Review on the Design and Hydration Properties of Natural Polymer-Based Hydrogels. *Materials* **2021**, *14*, 1095. [CrossRef] [PubMed]
78. Quodbach, J.; Preis, E.; Karkossa, F.; Winck, J.; Finke, J.H.; Steiner, D. Novel Strategies for the Formulation of Poorly Water-Soluble Drug Substances by Different Physical Modification Strategies with a Focus on Peroral Applications. *Pharmaceuticals* **2025**, *18*, 1089. [CrossRef] [PubMed]
79. Zhou, X.; Wang, Z.; Huang, H.; Liu, Y.; Li, S.; Qian, W.; Huang, S.; Xu, J. Entropy-mediated solidification stabilizes and enhances energetic release in amorphous energetic materials. *Nat. Commun.* **2026**, *17*, 3271. [CrossRef] [PubMed]
80. Surov, A.O.; Vasilev, N.A.; Vener, M.V.; Parashchuk, O.D.; Churakov, A.V.; Magdysyuk, O.V.; Perlovich, G.L. Pharmaceutical Salts of Fenbendazole with Organic Counterions: Structural Analysis and Solubility Performance. *Cryst. Growth Des.* **2021**, *21*, 4516–4530. [CrossRef]
81. Zakaria, M.Y.; Georghiou, P.E.; Banoub, J.H.; Beshay, B.Y. Inclusion of a Phytomedicinal Flavonoid in Biocompatible Surface-Modified Chylomicron Mimic Nanovesicles with Improved Oral Bioavailability and Virucidal Activity: Molecular Modeling and Pharmacodynamic Studies. *Pharmaceutics* **2022**, *14*, 905. [CrossRef] [PubMed]
82. Benkő, M.; Király, Z. Thermodynamics of inclusion complex formation of β-cyclodextrin with a variety of surfactants differing in the nature of headgroup. *J. Chem. Therm.* **2012**, *54*, 211–216. [CrossRef]
83. Belew, S.; Suleman, S.; Duguma, M.; Teshome, H.; Wynendaele, E.; Duchateau, L.; De Spiegeleer, B. Development of a dissolution method for lumefantrine and artemether in immediate release fixed dose artemether/lumefantrine tablets. *Malar. J.* **2020**, *19*, 139. [CrossRef] [PubMed]
84. Singh, B. A quantitative approach to probe the dependence and correlation of food-effect with aqueous solubility, dose/solubility ratio, and partition coefficient (Log P) for orally active drugs administered as immediate-release formulations. *Drug Dev. Res.* **2005**, *65*, 55–75. [CrossRef]

Disclaimer/Publisher's Note: The statements, opinions and data contained in all publications are solely those of the individual author(s) and contributor(s) and not of MDPI and/or the editor(s). MDPI and/or the editor(s) disclaim responsibility for any injury to people or property resulting from any ideas, methods, instructions or products referred to in the content.